

Liquid-Phase Exfoliation of Nonlayered Non-Van-Der-Waals Crystals into Nanoplatelets

Harneet Kaur and Jonathan N. Coleman*

For nearly 15 years, researchers have been using liquid-phase exfoliation (LPE) to produce 2D nanosheets from layered crystals. This has yielded multiple 2D materials in a solution-processable form whose utility has been demonstrated in multiple applications. It was believed that the exfoliation of such materials is enabled by the very large bonding anisotropy of layered materials where the strength of intralayer chemical bonds is very much larger than that of interlayer van der Waals bonds. However, over the last five years, a number of papers have raised questions about our understanding of exfoliation by describing the LPE of nonlayered materials. These results are extremely surprising because, as no van der Waals gap is present to provide an easily cleaved direction, the exfoliation of such compounds requires the breaking of only chemical bonds. Here the progress in this unexpected new research area is examined. The structure and properties of nanoplatelets produced by LPE of nonlayered materials are reviewed. A number of unexplained trends are found, not least the preponderance of isotropic materials that have been exfoliated to give high-aspect-ratio nanoplatelets. Finally, the applications potential of this new class of 2D materials are considered.

In most cases, 2D materials are based on layered crystals, a well-known material class consisting of strongly bonded atomic layers (or monolayers) which are stacked on top of each other, interacting via weak (usually van der Waals) interlayer forces.^[2] Well-known examples of layered crystals are graphite and transition metal dichalcogenides.^[1–3] Generally, 2D materials consist of one or more stacked monolayers and can be fabricated by bottom-up methods such as chemical synthesis,^[10] or vapor growth,^[11–13,14] as well as top-down methods which are generally referred to as exfoliation.^[4,5,15–17]

In bottom up-methods, small molecular building blocks undergo chemical reactions to grow 2D materials in solutions^[10,18] or on substrates.^[11–13,14] For substrate growth, chemical vapor deposition (CVD),^[11,12,19] pulse laser-deposition,^[13,19,20] metal–organic chemical vapor deposition (MOCVD),^[11,21] and molecular beam epitaxy^[12,14] are common methods.


However, top-down exfoliation is most relevant here and refers to the separation of 2D (or quasi-2D) fragments, often called nanosheets, from a layered crystal. Exfoliation is generally thought to be enabled by the highly anisotropic bonding scheme associated with layered materials where the weak interlayer interactions facilitate the removal of layers from the parent crystal.^[4–6,15,16,22–28] The earliest exfoliation process was micro-mechanical-cleavage^[1,7,29] which although useful was not scalable.^[30]

To achieve large-scale exfoliation, several scalable top-down exfoliation methods have been developed. Although it is possible to do large-scale exfoliation in a dry environment, for example by solid phase ball milling,^[31] most large-scale exfoliation is done in liquids. Of these, liquid-phase exfoliation (LPE) is possibly the most widely used top-down method to produce nanosheets from various layered materials.^[4–6,15–17,22–28] LPE involves injecting energy into appropriate liquids to induce fragmentation and delamination of atomic layers from their bulk layered counterparts.^[32] Energy is most commonly inputted into the dispersion via ultrasonication,^[33] although other methods such as microfluidization,^[34] wet ball milling,^[35] high shear mixing,^[36] homogenization,^[6,16,37,38] or wet-jet milling,^[33,35,39,40] have been used. This method has been used in the exfoliation of a wide variety of layered materials such as graphite, h-BN, black phosphorus, MoO₂, Ni(OH)₂, TMDs, GeS, SnP₃, etc.^[6,15,23,25,33,36,41–47] The liquid dispersions produced by LPE can have concentrations exceeding 1 g L⁻¹

1. Introduction

In the broadest sense, 2D materials are a form of matter defined by geometry, such that they display 1D (i.e., the thickness) that is extremely thin, sometimes atomically thin, while the other two dimensions display lateral sizes which are much larger than the thickness. Research into 2D materials became widespread following the discovery and initial characterization of graphene in 2004 and gradually grew to encompass a wide range of 2D materials.^[1–7] These materials have generated much excitement in the research community due to their combination of unusual properties,^[8] and exciting potential for applications.^[9]

H. Kaur, J. N. Coleman
School of Physics
CRANN & AMBER Research Centres
Trinity College Dublin
Dublin D02 PN40, Ireland
E-mail: colemaj@tcd.ie

 The ORCID identification number(s) for the author(s) of this article can be found under <https://doi.org/10.1002/adma.202202164>.

© 2022 The Authors. Advanced Materials published by Wiley-VCH GmbH. This is an open access article under the terms of the Creative Commons Attribution License, which permits use, distribution and reproduction in any medium, provided the original work is properly cited.

DOI: 10.1002/adma.202202164

and contain nanosheets with a broad distribution of lateral size and thickness.^[25,47] For example, for MoS₂ the lateral size has been reported to vary from 40–400 nm with a thickness range of 1–10 atomic layers.^[48] The distribution of the dimensions is linked to nanosheet mechanics; therefore, the range of size and thickness is different for different layered materials.^[49,50] It is worth noting that LPE is distinct from other liquid exfoliation methods such as graphene-oxide-based exfoliation as it involved no chemical modification of the material before, during, or after exfoliation.

A significant advantage of solution-based exfoliation methods is that the as-produced dispersions can easily be converted to inks which can be readily printed on various substrates for applications in electronics,^[51] energy generation and storage,^[42,46,52] sensing,^[53,54] and biomedicine.^[55]

It is probably fair to say that most researchers initially expected LPE to be strongly limited to layered materials due to the relative ease with which weak interlayer interactions can be broken. However, the work of the Gogotsi group on MXenes^[56] showed that 3D nonlayered crystals could be chemically converted to layered crystals which can then be exfoliated using LPE. This work has spawned a field which is based on the exfoliation of MAX phases, that is transition metal carbides or nitrides with the general formula, M_{n+1}AX_n (*n* = 1–3),^[56–60] where, M is an early transition metal (Ti, V, Cr, etc.), A is group 13 or 14 elements (Al, Si, etc.), and X is either carbon or nitrogen.^[57,60,61] The MAX phases can be chemically modified by selectively etching the A atoms,^[59,61,62] resulting in a layered structure of MX slabs held together by weak residual forces,^[57,59,61–63] the so-called MXenes.^[57,59,62] These weak forces can then be easily broken by LPE to produce individual nanosheets due to high mechanical anisotropy in the MXenes.^[57,62]

Although it is essentially a two-step process (etching followed by exfoliation), the production of MXenes can be considered as a type of LPE because at the moment of exfoliation the material is a layered crystal consisting of well-defined layers bonded by weak interlayer interactions. However, the case of MXenes is thought-provoking: could nonlayered crystals which display strong bonding in all three directions and no van der Waals gap be directly exfoliated into nanosheets using LPE (i.e., cutting out the etching step)?

In fact, the answer turned out to be yes. In 2017, a paper by Guan et al.^[64] demonstrated that monoclinic tungsten trioxide (α -WO₃) crystals can be exfoliated into nanoplatelets by the LPE process. Here, we use the term nanoplatelets to refer to the 2D-fragments produced from the LPE of nonlayered compounds whereas we use nanosheets to refer to 2D objects produced by the exfoliation of layered compounds. Unlike MoO₃, WO₃ is a nonlayered, non-van der Waals (NL-NvdW) material that displays strong bonding in all three dimensions. To our knowledge, this is the first example of LPE of such a 3D-crystal leading to the production of nanoplatelets. At roughly the same time, another paper by Tai et al.^[65] demonstrated the production of nanoplatelets from LPE of olivine type LiFePO₄, and spinel-type LiMn₂O₄. We want to emphasize here that both these crystals are strongly bonded and nonlayered. Although 2D-nonlayered nanoplatelets have been synthesized in the past by using different chemical routes,^[66,67] but this direct LPE using a nonlayered 3D-compound as a starting material is surprising.

This result was followed by the successful LPE of various other nonlayered strongly bonded crystals^[68–86] into nanoplatelets: β -boron,^[86–90] α -Fe₂O₃,^[68] MnTe,^[71] Si,^[73,78] PbS,^[75] FeS₂,^[79,81,82] α -Ge,^[77,84,91] Sn,^[83] B₄C,^[85] etc. These developments have raised many questions regarding the mechanism of the LPE process and the properties of the nonlayered 3D-strongly bonded materials which allow exfoliation by LPE by using them directly as starting materials.

As described by several authors,^[32,92,93] LPE of layered materials involves breaking a combination of weak interlayer and strong intralayer bonds. Indeed, it is the significant difference in the strength of intra- versus intersheet bonds that leads to the relatively large aspect ratios of exfoliated nanosheets which range from \approx 100 to $<$ 10.^[49,50] However, as nonlayered 3D-crystals are strongly bonded in all directions, the only process that can lead to exfoliation is the rupturing of chemical bonds. This raises several questions: why does LPE of nonlayered 3D-crystals lead to nanoplatelets, as evidenced by recent publications, and not 3D or quasi-0D nanoparticles? Can all 3D-strongly bonded nonlayered crystals be exfoliated by LPE resulting in nanoplatelets? If not, what are the selection criteria? What energy input and solvent vehicles are most appropriate? These questions must be answered if we want to fully utilize the potential for new nanomaterials discovery offered by the ability to directly exfoliate nonlayered 3D-crystals.

Several comprehensive reviews on LPE of layered materials have been published in the literature.^[5,16,32,45,48,53,94] Here, our goal is to present an overview and perspective on the use of the LPE process for NL-NvdW 3D-bonded crystals for the production of nanoplatelets. The manuscript consists of a very brief description of the general LPE process, followed by a detailed survey of most of the 3D-bonded NL-NvdW crystals that have been directly exfoliated into nanoplatelets by LPE. These 3D-crystals considered in this study are further divided into anisotropic and isotropic, based on the bonding scheme. Furthermore, the structure and aspect-ratio of obtained nanoplatelets, as well as cleavage plane directions and liquid media used in LPE, are discussed. We have also briefly discussed the applications of these materials and given our view on the challenges and prospects. We anticipate that this manuscript will provide inspiration for the synthesis of other novel NL-NvdW nanoplatelets, possibly leading to novel applications. In addition, we hope it will encourage readers to answer the questions listed above in order to further our understanding of this interesting topic.

2. A Brief Introduction to Liquid-Phase Exfoliation (LPE)

The liquid-phase exfoliation method was originally developed to produce graphene in large quantities in 2008.^[16,43] It is based on the principle that conversion of a layered crystal to large quantities of nanosheets in liquids requires two stages: the breaking of bonds to separate the nanosheets from the crystal and stabilization of the resultant nanosheets against reaggregation.

In order to separate the nanosheets from the parent crystal, it is necessary to pump energy into the exfoliation liquid. Although this can be done in a range of ways, including for

example heating reflow exfoliation^[95] and microwave exfoliation,^[96] LPE can be divided into the following major categories:

2.1. Sonication

There are two types of sonication: bath sonication and probe sonication. In bath sonication, ultrasonic waves through the water induce pressure oscillations which in turn result in the growth and collapse of microbubbles resulting in powerful shockwaves and locally high shear rates.^[48,97] This sonicated power is transferred to the vial placed in the bath, containing the 2D-material in liquid media. Whereas, in probe sonication, a sharp tip (probe) is placed directly within the liquid media in a vial. Fragmentation and delamination result in the production of nanosheets in both processes,^[32,48] but the power in probe sonication is often larger than a bath partly because the power supply given by the probe is larger as compared to a bath. In addition, the probe is in direct contact with the sample, while in the bath, the sample is spatially separated from the energy source.

2.2. Shear Exfoliation

Here, the material is exfoliated by exposure to shear forces in a suitable liquid media. Usually, the shear is applied in a turbulent system, leading to very high local shear rates.^[24] The collision of particles can cause fragmentation while the shear forces cause slide off of nanosheets from the parent crystal. It is mainly executed by either using a high-shear mixer^[36] or by microfluidization,^[98] homogenization,^[38] and wet-jet milling.^[39]

2.3. Cryo-Mediated Sonication

In this somewhat less common process, liquid nitrogen is used during or prior to the sonication process to induce cracks in the bulk structure.^[99] It can be of two types: crystals are pre-treated in liquid nitrogen prior to sonication in a liquid media, or the crystals suspended in the liquid media are frozen first by using liquid nitrogen followed by a sonication process. Either way, such low temperatures result in cracks in the bulk material, which along with sonication, results in the production of nanosheets.^[99]

It must be emphasized that the removal of nanosheets from a layered crystal requires the breaking of both weak-interlayer bonds and strong intralayer bonds. Recent work^[32,49] has shown that experimental data on the distribution of nanosheet sizes in dispersions produced by LPE can be explained under the assumption that equal energy goes into breaking weak-interlayer bonds as is used to break strong intralayer bonds. As a result, the achieved nanosheet aspect ratio (ratio of lateral size to thickness) is strongly related to the ratio of intra- to interlayer bonding strengths.^[49]

Stabilization is generally achieved either by careful choice of the solvent in which the exfoliation is performed or by adding stabilizing additives to the exfoliating solvent. It has been shown, both experimentally and theoretically, that the most effective

solvents for stabilization are those with the same surface energy as the nanosheets to be stabilized.^[6,36,43,100] Probably the most commonly used solvent is *N*-methyl-2-pyrrolidone,^[6,16] although many other organic solvents such as *N,N*-dimethylformamide (DMF), ortho-dichlorobenzene, and *N*-cyclohexyl-2-pyrrolidone have suitable surface energies.^[6,23,27] However, many surface-energy matched solvents have high boiling points and are toxic which makes them unattractive. To address this, the Zhang group has used a mixture of two low-boiling point solvents ethanol/water and demonstrated that the mixture has surface energy close to NMP, and successfully achieved exfoliation of MoS₂ and WS₂.^[101] Alternatively, it is possible to exfoliate in NMP and then solvent-exchange to more benign solvents such as isopropanol.^[4,102] Similar to solvent exfoliation, LPE has been achieved in ionic liquids such as 1-butyl-3-methylimidazolium bis(trifluoromethylsulfonyl) imide ([Bmim][Tf₂N]) or 1-hexyl-3-methylimidazolium hexafluorophosphate (HMIM).^[103]

Additives have also been employed in the LPE procedure to achieve stable dispersions in environmentally benign solvents such as aqueous solutions of surfactants such as sodium deoxycholate (DOC), sodium dodecyl sulfate (SDS), poly (sodium 4-styrenesulfonate) (PSS), etc.,^[28,104] or polymer solutions such as poly(vinyl chloride) (PVC), poly(methyl methacrylate) (PMMA), ethyl cellulose, etc.^[23,27,105]

In terms of stabilizing additives, it is very common to use surfactants or polymers to add a stabilizing coating to the nanosheet preventing aggregation either via electrostatic^[106] or steric stabilization,^[107] respectively. Surfactant stabilization has been used to disperse a range of nanosheet types.^[108] One significant advantage of using surfactants is that they facilitate the fabrication of aqueous dispersions allowing all the inherent advantages of using water as a solvent. For example, large-scale exfoliation is generally performed in water using surfactants.^[36] Although additives result in enhanced dispersibility and stability, it is difficult to completely remove them to obtain the pristine form of nanosheets after exfoliation.^[28,48] This can lead to some problems when fabricating materials for some applications.

3. LPE of Nonlayered Non-van-der-Waals (NL-NvdW) Compounds

3.1. Recent Trends from the Literature

Figure 1A shows the number of publications reported on the production of nanoplatelets from NL-NvdW 3D-bonded crystals by the LPE method as a function of publication year. The first use of LPE beyond layered materials occurred in 2017 with the exfoliation of tungsten trioxide (α -WO₃) into nanoplatelets,^[64] followed by the exfoliation of lithium manganese oxide (LiMn₂O₄), and lithium iron phosphate (LiFePO₄) in the same year.^[65] Subsequently, new publications appeared each year as shown in Figure 1A.

One important factor which should determine whether exfoliation yields 2D-nanoplatelets is the anisotropy of bonding. It has been proposed that the aspect-ratio of 2D nanosheets is related to the bonding anisotropy which can be represented by surface energy anisotropy.^[49] The surface energy (γ) determines the equilibrium shape of the many nanoparticles

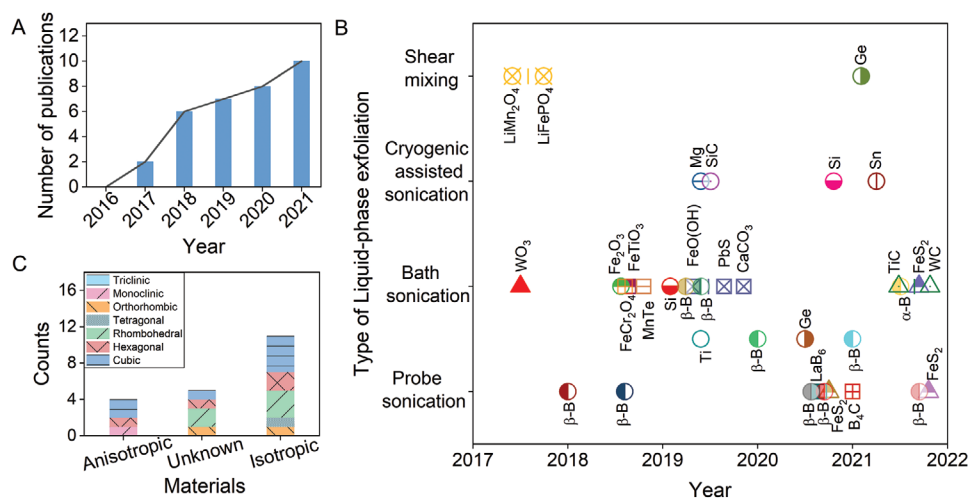


Figure 1. Progress in the use of LPE process to produce nanoplatelets from NL-NvdW materials. A) Number of publications reported on the use of LPE process in exfoliation of NL-NvdW crystals versus year of publication. B) An exhaustive list of all NL-NvdW crystals exfoliated by LPE by different research groups until 2021. The graph is divided on type of LPE process used in exfoliation versus the publication year. The crystals were divided with respect to the variation in the value of surface energies (γ) as anisotropic (represented by triangle symbol) and isotropic (represented by circles). The crystals for which the information on γ is unknown is represented by the square symbol. The same material exfoliated by different research groups is represented with the same symbol but with a different color scheme. C) Histogram representing the number of mechanical anisotropic, isotropic, and unknown crystals exfoliated by LPE. The different color/pattern among each stack represents different crystal lattice system. Boron carbide B_4C is not included in (C), because it has icosahedral crystal structure.

and mesoscopic crystals as it is a measure of the surface excess free energy per unit area of a particular crystal facet.^[109,110] Since it relates to the strength of the atomic bonds and atomic densities of a particular atomic plane, its value is different for different facets.^[109–111] The higher the γ value for a particular facet, the less easily it is anticipated to cleave, and the easiest facet to cleave is the one with a minimum value of γ .^[111] For a perfect isotropic crystal, the value of γ for all facets should ideally be similar.^[110] However, many crystals are somewhat anisotropic such that the variation in the value of γ can be used as a general measure of anisotropy.^[110] To our knowledge, there is no well-defined criterion that determines whether a crystal is isotropic or anisotropic. Therefore, for the purposes of this work, we propose that anisotropic crystals are those where the most strongly bonded atomic plane has surface energy which is at least a factor of three greater than that of the most weakly bonded plane. Thus, we define a factor, $\chi = \gamma_{\text{max}}/\gamma_{\text{min}}$ which is >3 for anisotropic crystals and ≤ 3 for isotropic crystals (refer to Table S1, Supporting Information, for γ values).

Based on this definition, we plot a graph showing all exfoliated NL-NvdW crystals classified by the exfoliation method used in LPE, and the crystal type (isotropic or anisotropic based on χ) as shown in Figure 1B. Anisotropic and isotropic crystals are represented by triangles and circle symbols respectively while, for crystals for which γ values are unknown, a square symbol is used to represent the crystal.

Based on the predictions of ref. [49] liquid exfoliation of crystals with intrinsic bonding anisotropy might be expected to yield quasi-2D nanosheets, similarly to layered materials, while isotropic crystals should not. However, based on our analysis of χ , we found only 4 materials out of 23 different NL-NvdW crystals exfoliated by LPE which possess some intrinsic mechanical anisotropy. Surprisingly, 11 NL-NvdW crystals were isotropic

(refer to Table S1, Supporting Information), with the remaining 8 of unknown anisotropy. As observed in Figure 1B, the earliest example of LPE of NL-NvdW compounds was for a crystal with intrinsic mechanical anisotropy, α - WO_3 .^[64] However, very quickly LPE of many isotropic crystals such as LiMn_2O_4 ,^[65] α - Fe_2O_3 ,^[68] SiC ,^[76] Si ,^[73,78] Mg ,^[74] α - Ge ,^[77,84,91] Sn ,^[83] etc. was demonstrated. We feel that this preponderance of isotropic materials exfoliated by LPE is very unexpected and raises questions about the nature of the exfoliation mechanism.

Also, as it can be seen in Figure 1B, bath sonication is the most common type of LPE procedure adopted by research groups. It has been used in the exfoliation of a list of materials such as α - WO_3 ,^[64] β -B,^[88,112] α - Fe_2O_3 ,^[68] FeTiO_3 ,^[69] FeCr_2O_4 ,^[70] MnTe ,^[71] Si ,^[73] α - FeO(OH) ,^[75] PbS ,^[75] CaCO_3 ,^[75] FeS_2 ,^[82] TiC ,^[113] WC ,^[113] and α -B.^[114] One point to note here is that this list includes all the four anisotropic crystals: α - WO_3 ,^[64] FeS_2 ,^[82] TiC ,^[113] and WC ,^[113] (see Table S1, Supporting Information).

On the other hand, most of the highly isotropic crystals ($\chi \approx 1$ –1.6) such as Ti ,^[72] Mg ,^[74] Ge ,^[77] Sn ,^[83] and SiC ^[76] were either exfoliated using cryogenic assisted exfoliation or by incorporating probe sonication during the process. Cryogenic exfoliation is performed at very low temperatures by using liquid nitrogen during the sonication process.^[74,76,83] It may be that the generation of cracks during the cryo-treatment is an important factor in the exfoliation of isotropic NL-NvdW materials while the high energy densities associated with probe sonication may be important.

The least common process used is shear exfoliation. This has only been reported by two groups: Tai et al.^[65] in the exfoliation of LiMn_2O_4 , and Gibaja et al.^[84] in the exfoliation of α - Ge . In fact, as shear exfoliation is a relatively low energy process,^[36] it is perhaps surprising that it can be used to exfoliate isotropic NL-NvdW materials at all.

Certain crystals such β -B,^[86–90,112,115–118] FeS₂,^[79,82] Si,^[73,78] and Ge^[77,84] have been exfoliated by various research groups using multiple methods of LPE. This has resulted in different yields and dimensions of the exfoliated products as discussed in the next sections.

Figure 1C shows a histogram depicting that more isotropic crystals are exfoliated to date as compared to the anisotropic ones among the classification. Even if all the unknown materials turned out to be anisotropic, isotropic materials would still make up roughly half of the total cohort. The histogram further gives information onto the type of the crystal lattice structure of different materials considered in this review, representing most of the materials exfoliated so far possess cubic crystal lattice structure.

Based on the electronic properties we have also observed that most of the material exfoliated are semiconductors, such as α -WO₃,^[64,119] LiMn₂O₄,^[65,120] β -B,^[121,122] α -Fe₂O₃,^[68,123] FeCr₂O₄,^[70,124] FeTiO₃,^[69,125] MnTe,^[71] PbS,^[75,126] α -FeO(OH),^[127] SiC,^[76] B₄C,^[128] FeS₂,^[79,123] Ge,^[129] Si,^[129] TiC,^[130] and WC.^[131] This is very important because all these materials are fundamentally different, as semiconductors such as silicon, germanium, etc. have highly directional bonds,^[132] whereas metallic crystals such as magnesium, titanium, etc. have the highest isotropy due to the presence of directionless metallic bond between the atoms.^[133]

3.2. Lattice Structure

The lattice structure of NL-NvdW crystals is distinct from layered materials due to the presence of strong bonds in all the three-directions. To exfoliate nonlayered materials, the strong bonds must be broken. **Figure 2** shows some important examples of NL-NvdW materials exfoliated by LPE which are arranged in the order of year of publication. The atomic arrangement of atoms in the crystal lattice structure, transmission electron microscopy (TEM) images of the exfoliated products, and high-resolution TEM (HRTEM) or scanning transmission electron microscopy (STEM) images are shown for each example in Figure 2.

In 2017, α -WO₃ was exfoliated using commercial source powder as the starting material.^[64] As shown in Figure 2, it has a monoclinic lattice structure belonging to the P21/n space group.^[64] The exfoliated products were characterized with TEM which confirmed its 2D-morphology, and HRTEM images displaying two sets of lattice fringes with *d*-spacing of 0.36 and 0.38 nm, which is assigned to the (200) and (020) planes of monoclinic α -WO₃, confirmed its structure.^[64] During the same time, exfoliation of Li-storing materials such as LiMn₂O₄ was also reported.^[65] In this case, the starting material was synthesized, and characterized by X-ray diffraction (XRD) prior to exfoliation.^[65] XRD confirmed the spinel structure of LiMn₂O₄ belonging to the Fd3m space group (cubic lattice structure).^[65] After exfoliation, TEM studies showed the exfoliated products consist of several layers, and the HRTEM image showed lattice fringes with a spacing of 0.47 nm, which is assigned to the (003) plane of the spinel crystal structure of LiMn₂O₄.^[65]

The first mono-elemental NL-NvdW material, β -boron was also exfoliated in 2018.^[86] Boron forms complicated crystal structures based on icosahedral B₁₂ clusters.^[86,121] These clusters

link into rigid frameworks, and forms four stable phases at ambient conditions: α -rhombohedral boron, β -rhombohedral boron, γ -orthorhombic boron, and β -tetragonal boron.^[121,134] β -rhombohedral boron (β -B) is the most common and stable phase, which has been used by many research groups as the starting material in the exfoliation to produce nanoplatelets.^[86–90,112,115–118] The TEM image of the exfoliated product shows nanoplatelets, and fringe spacing of 0.504 nm in HRTEM image was assigned to the (104) plane of the β -rhombohedral boron structure.^[86]

In the same year, for the first time, exfoliation using a natural mineral ore of NL-NvdW compound as a starting material is used in LPE as demonstrated by the Ajayan group.^[68] Hematite mineral (α -Fe₂O₃) was used in the exfoliation.^[68] It has a rhombohedral crystal system, R $\bar{3}c$ space group.^[68] The TEM images showed the presence of 2D-hematene, and the STEM image showed the atomic structure in the [001] orientation of the flake.^[68] This work is then followed by the exfoliation of many other minerals such as chromite,^[70] ilmenite,^[69] goethite,^[75] galena,^[75] calcite,^[75] and pyrite.^[81,82]

Titanium is the first early transition metal to be exfoliated in 2019.^[72] Commercial source α -Ti powder with hexagonal crystal structure was used in the exfoliation.^[72] Nanoplatelets of lateral dimensions of 50–100 nm were observed in TEM images, and lattice spacing of 0.24 and 0.26 nm is found in the HRTEM image.^[72] Alkaline-earth metal, magnesium is also exfoliated around the same time.^[74] The crystal structure of bulk Mg is hexagonal.^[74] The TEM image showed its successful exfoliation, although it was observed that the produced nanoplatelets were oxidized,^[74] but the bulk of the platelets are mainly composed of metallic Mg as confirmed by the HRTEM image showing the hexagonal lattice structure of magnesium atoms in the platelets as shown in Figure 2.^[74]

In 2020, the first NL-NvdW TMD, FeS₂ is exfoliated by us.^[79] We used a commercially sourced powder with a cubic crystal lattice structure as a starting material in the exfoliation experiment. It is confirmed by TEM images, that the exfoliated products have 2D-morphology.^[79] The STEM image from a 2D-platelet showed lattice spacing of 0.31 and 0.19 nm, assigned to the (111) and ($\bar{2}20$) miller index of the cubic crystal lattice structure of FeS₂.^[79]

Around the same time, silicon, a group 14 semiconductor with cubic crystal lattice structure was exfoliated using commercial sourced silicon powder.^[78] TEM images showed the 2D-nature of the exfoliated product, and HRTEM showed lattice spacing of 0.19 nm, assigned to the (111) planes of the cubic crystal lattice structure of silicon.^[78] We want to mention here that the first claims of silicon exfoliation were published in 2019^[73] but no structural analysis was done by the authors.^[73] Other group 14 elements were also exfoliated afterward^[77,83,84] such as germanium,^[77,84] and tin^[83] as shown in Figure 2. Both have cubic crystal lattice structures and the exfoliated products showed 2D-nature with the crystal structure of bulk as confirmed with STEM in case of Ge^[84] and HRTEM in Sn platelets.^[83] Even transition metal carbides, such as TiC, which is known for their extreme hardness were also successfully exfoliated by LPE, and structurally characterized by TEM which confirmed the 2D-morphology and bulk cubic lattice structure of the exfoliated platelets is confirmed with HRTEM.^[113]

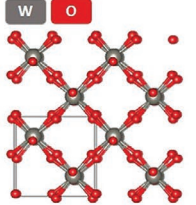
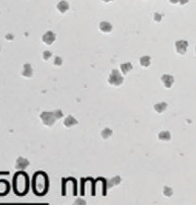
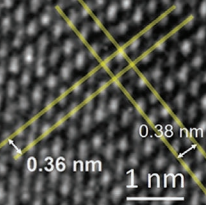
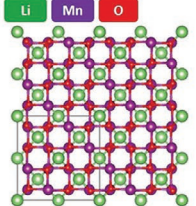
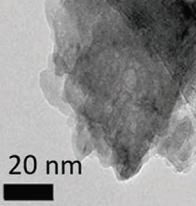
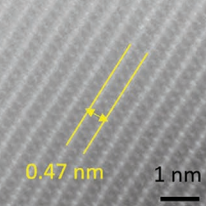
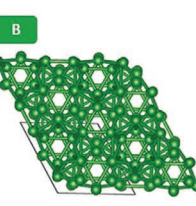
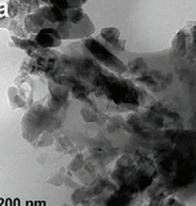
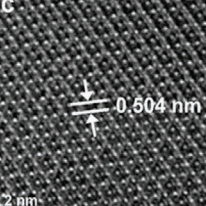
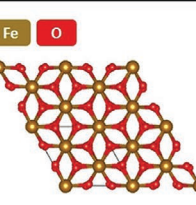
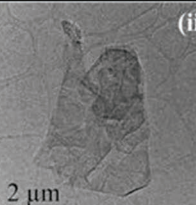
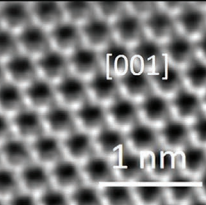
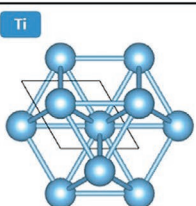
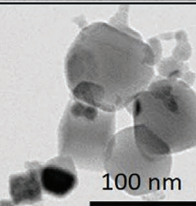
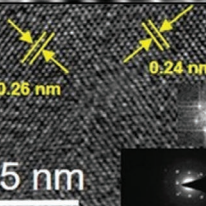
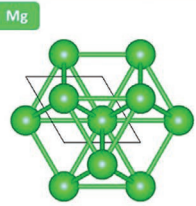
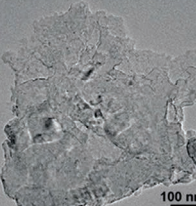
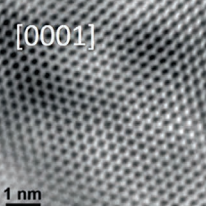
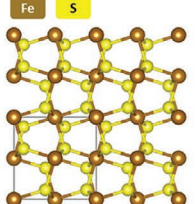
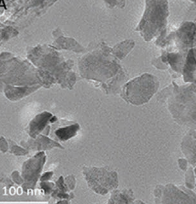
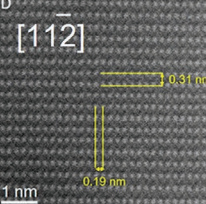
Name Lattice System Year of exfoliation	Crystal Structure	TEM image	HR-TEM/ STEM image
Tungsten oxide (WO ₃) Monoclinic 2017			
Lithium Manganese dioxide (LiMn ₂ O ₄) Cubic 2017			
Boron (β-B) Rhombohedral 2018			
Hematite (α-Fe ₂ O ₃) Rhombohedral 2018			
Titanium (α-Ti) Hexagonal 2019			
Magnesium (Mg) Hexagonal 2019			
Pyrite (FeS ₂) Cubic 2020			

Figure 2. Examples of the NL-NvdW materials exfoliated by LPE process. The materials are arranged in the order of year of publication. The name of the material, its lattice structure, and year of the publication are mentioned in column 1. The arrangement of atoms in the crystal lattice is shown in column 2.

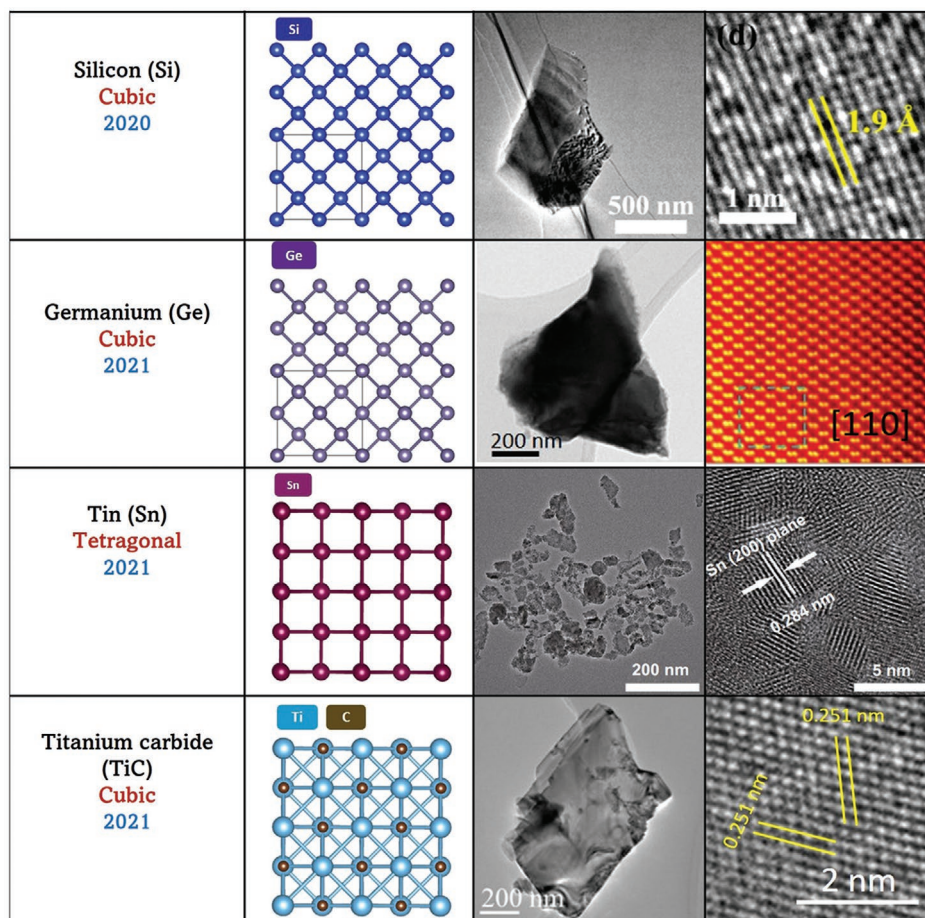


Figure 2. Continued.

The projection vector of all the atomic models is [001]. The TEM-image of the exfoliated products are shown in column 3, and the corresponding HRTEM, or STEM images are shown in column 4. Monoclinic α - WO_3 is the first NL-NvdW crystal to be exfoliated. Reproduced with permission.^[64] Copyright 2017, Wiley-VCH. This is followed by LPE of cathode materials for the batteries, for example, LiMn_2O_4 . Reproduced with permission.^[65] Copyright 2017, Wiley-VCH. β -Boron with rhombohedral crystal lattice structure is the first mono-elemental NL-NvdW material to be exfoliated in 2018. Reproduced with permission.^[86] Copyright 2018, American Chemical Society. This is followed by hematite, first NL-NvdW crystal to be exfoliated using its mineral ore in 2018. Reproduced with permission.^[68] Copyright 2018, The Authors, published by Springer Nature. In 2019, first transition metal titanium is exfoliated, Reproduced with permission.^[72] Copyright 2019, American Chemical Society. This is followed by exfoliation of alkali-earth metal, magnesium. Reproduced with permission.^[74] Copyright 2019, Wiley-VCH. In 2020, first NL-NvdW disulfide, FeS_2 is exfoliated. Reproduced with permission.^[79] Copyright 2020, American Chemical Society. In the same year, group 14 semiconductor, silicon is exfoliated. Reproduced with permission.^[78] Copyright 2020, American Chemical Society. This is followed by other members of group 14 elements, exfoliation of germanium and tin. Germanium: Reproduced with permission.^[84] Copyright 2021, Wiley-VCH. Tin: Reproduced under the terms of the CC-BY Creative Commons Attribution 4.0 International license (<https://creativecommons.org/licenses/by/4.0>).^[83] Copyright 2021, The Authors, published by Springer Nature. Lastly, first transition metal carbide such as TiC is exfoliated in 2021. Reproduced with permission.^[113] Copyright 2021, Wiley-VCH. In the above, only the TEM and HRTEM/STEM images in columns 3 and 4 are reproduced from the respective quoted references.

All these different examples indeed prove that nanoplatelets can be produced from exfoliation of a range of different NL-NvdW materials, with distinct lattice structures, and show that the resultant crystal structure of the exfoliated nanoplatelets is similar to its bulk structure. But the important question which is not addressed here is: how 2D are these nanoplatelets? TEM is a high-throughput technique that provides information about the lateral size of nanoplatelets such as length and width. But unfortunately, TEM is not usually able to provide information about nanoplatelet thickness. However, atomic force microscopy (AFM) measurements can be used to obtain

statistical data on the nanoplatelet thickness distribution. Such measurements are crucial to truly assess the nanoplatelet geometry and identify how 2D these nanoplatelets really are as discussed in the next section.

3.3. Quantification of the 2D-Nature of the Nanoplatelets

When 2D materials are produced by any liquid exfoliation process, it is critically important to measure the dimensions of the resultant nanosheets or nanoplatelets. Knowledge of the

nanosheet length, width, and thickness has previously proved important for both understanding the exfoliation mechanism^[49] as well as quantifying the performance of nanosheets in applications.^[135] This is particularly important with the LPE of non-layered compounds, especially those with isotropic bonding schemes. This is because the ability to exfoliate such materials is somewhat unexpected, putting the onus on the researcher to unambiguously prove the 2D nature of the resultant particles.

The best way to measure the dimensions of ensembles of nanosheets or nanoplatelets is via statistical AFM.^[48,49] However, this process can be more challenging than is often appreciated. For example, with liquid exfoliated layered materials, it is well established that AFM measures an apparent nanosheet thickness with an internal calibration required to establish the real thickness.^[48,136,137] In addition, if a dispersion has a very broad distribution, AFM analysis can be affected by an observational bias, either due to limited scan size of the AFM or failure to measure a representative sample within the ensemble. This problem can be minimized by first size-selecting the dispersion,^[137] and then performing AFM on various fractions.^[48] In addition, as we have described earlier,^[48] for AFM data to be reliable it is very important to analyze at least 100–150 individual nanosheets to obtain good population histograms. If the imaging and counting are unbiased, the histogram is generally close to a log-normal distribution. It is also important to avoid counting those aggregates that appear to have formed during drying. Once this is achieved, statistical analysis can be performed—for example, the average nanosheet length, width, and thickness can be extracted with acceptable errors.^[48]

Moreover, extreme care must be taken to ensure that the 2D objects in the AFM images which are being analyzed are actually nanosheets and not artifacts, for example, patches of dried solvent or surfactant. Readers would be surprised to know how often papers purporting to show AFM images of high aspect-ratio nanosheets are actually reporting solvent or surfactant patches. The easiest way to avoid this is to measure length histograms by using both TEM and AFM and check that they are similar (within the difference expected due to tip convolution effects). Alternatively

correlating AFM with scanning of Raman (or sometimes PL) spectra can confirm the identity of the observed 2D objects.

To quantify the 2D-nature, it is important to measure the nanosheet aspect ratio, α , which is usually defined as the ratio of nanosheet length (measured as the largest lateral dimension), L , to thickness, t : $\alpha = L/t$. Ideally, α is measured by AFM on a platelet-by-platelet basis allowing it to be represented in various ways. By definition, for a platelet, $L > t$, that is, $\alpha > 1$ with larger values of α indicating greater 2D-character. Depending on the material, nanosheets obtained from LPE of layered materials typically show lengths between 20 to 1000 nm and thicknesses between 0.35 to 20 nm.^[49] In general, the highest mean aspect ratios observed for layered nanosheets produced by LPE are ≈ 50 (for graphene) with layered hydroxides displaying aspect ratios as low as ≈ 5 , with aspect ratio directly linked to bonding anisotropy.^[49] Given the limited anisotropy associated with NL-NvdW materials, one would expect the observed aspect ratios to be at the lower end of this range.

We have made a list of NL-NvdW materials (shown in Table 1) for which a reasonably large sample set (>50) of platelets was analyzed by AFM. Unfortunately, there are relatively few materials for which such a complete set of analyses is done. We have also given information in Table 1 about the method of LPE, liquid-media, and centrifuge speed used by the researchers in the experiments, as all these parameters affect the aspect-ratio of the platelets. As observed in Table 1, centrifugation was employed by all of them to size separate the exfoliated platelets in the as-obtained dispersion. However, in different papers the centrifuge speeds were quoted in different units; revolution per minute (rpm), and in relative centrifugal force (g). It is very important to note that rpm is not an appropriate unit to report as a given rpm produces different g-force in different centrifuge setups. Therefore, we want to emphasize here, that only the units given in g-force can be compared to each other. We have also estimated the $\langle L \rangle$ by taking the square root of the average area of platelets for which the $\langle L \rangle$ is not given in the publications.^[85,86] This helps us to estimate the approximate mean value of $\langle \alpha \rangle$ by taking the ratio of $\langle L \rangle / \langle t \rangle$.

Table 1. List of materials for which a finite sample size of nanoplatelets was analyzed with AFM. The list shows the name of the materials (column 1), method used in LPE (column 2), the type of liquid media used (column 3), number of nanoplatelets counted by AFM (column 4), centrifuge-speed used to size select the platelets (column 5), average length obtained by AFM ($\langle L \rangle$, column 6), average thickness obtained by AFM ($\langle t \rangle$, column 7), aspect-ratio ($\langle \alpha \rangle = \langle L \rangle / \langle t \rangle$, column 8), and the respective reference (column 9). The units of centrifuge speed are in 10^3 revolutions per minute (krpm) or 10^3 -g-force (kg).

Materials	Method	Liquid-media	Sample size	Centrifuge speed	$\langle L \rangle$ [nm]	$\langle t \rangle$ [nm]	α	Ref.
FeS ₂	Probe sonication	NMP	100	0.025–0.22 kg	234 ± 9	59 ± 3.5	3.9	[79]
			100	0.22–0.63 kg	177 ± 4	43 ± 1.4	4.1	
			100	0.63–1.24 kg	137 ± 6	31 ± 2	4.4	
			100	1.24–2.06 kg	80 ± 3	18 ± 1	4.4	
B ₄ C	Probe sonication	IPA	169	5 kg	127	31.4	4	[85]
β -B	Probe sonication	IPA	180	≥ 5 krpm	44	4.7	9	[86]
		DMF	180	≥ 5 krpm	140	1.8	77	
α -WO ₃	Bath sonication	BSA in water, pH 4	100	2–5 krpm	–	2.5	–	[64]
			100	≥ 5 krpm	–	1.7	–	
α -Ge	Shear exfoliation	IPA:water (4:1)	≈ 57	≥ 3 krpm	1500	18.5	81	[84]
β -B	Solvothermal-assisted probe	Acetone	200	≥ 6 krpm	5050	3.5	1442	[115]

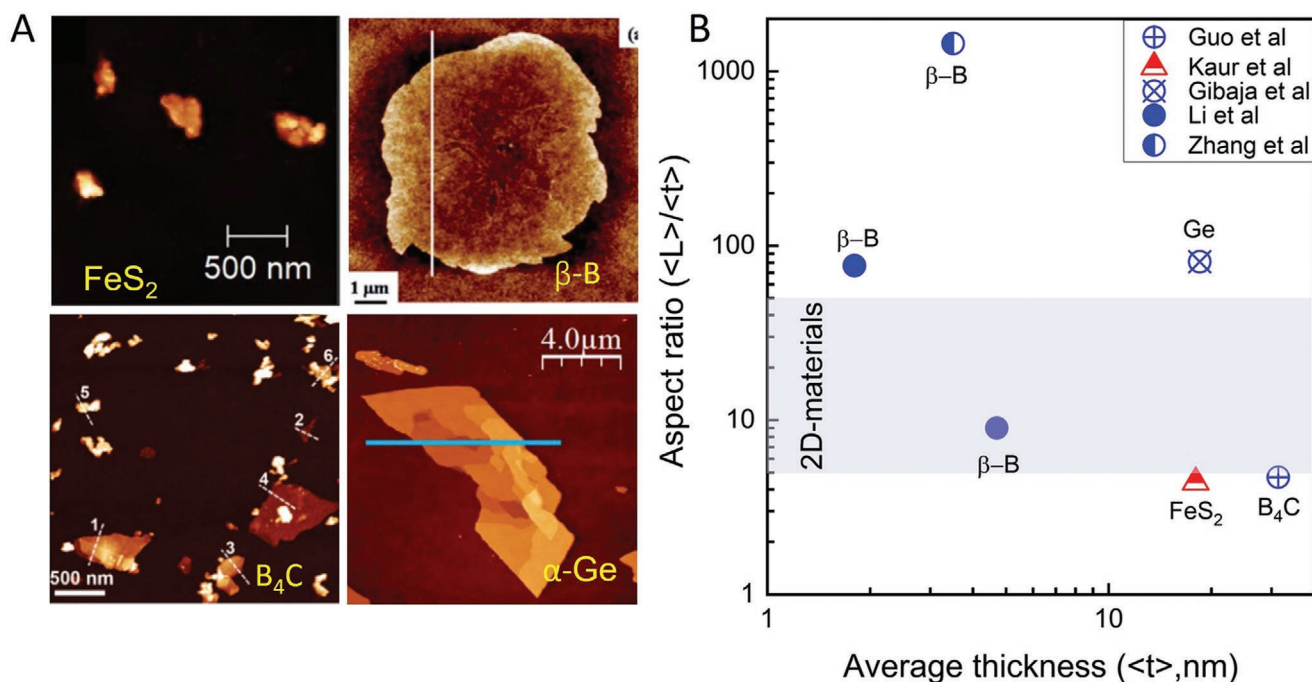


Figure 3. Atomic force microscopy images and comparison of the aspect ratio. A) AFM images of the LPE produced nanoplatelets of FeS₂, β-B, B₄C, and α-Ge. The name of the materials is mentioned in the respective AFM images. Image for FeS₂: Reproduced with permission.^[79] Copyright 2020, American Chemical Society. Image for β-B: Reproduced with permission.^[115] Copyright 2020, Royal Society of Chemistry. Image for B₄C: Reproduced with permission.^[85] Copyright 2021, Royal Society of Chemistry. Image for α-Ge: Reproduced with permission.^[84] Copyright 2021, Wiley-VCH. B) Plot of the aspect ratio (defined as the ratio of average length to average thickness) versus average thickness. Each data point represents a different NL-NvdW material. The triangular symbols represent the nanoplatelets obtained from exfoliation of mechanical anisotropic compounds, and the circular symbol represents the nanoplatelets obtained from LPE of isotropic compounds. The shaded region in the plot shows the range of the aspect-ratio of nanosheets obtained from the LPE of most of the layered materials.

To analyze Table 1, we have prepared **Figure 3** which shows AFM images of exfoliated nanoplatelets from an anisotropic crystal, FeS₂,^[79] and isotropic crystals, β-B,^[115] B₄C,^[85] and α-Ge,^[84] as well as a graph of the estimated value of $\langle \alpha \rangle$ plotted versus $\langle t \rangle$. The examples given in Figure 3A were specifically chosen for two main reasons: the platelets have a well-defined sharp edge in the AFM image and a reasonably high number of platelets were analyzed by the AFM with a complete set of analyses on $\langle L \rangle$ and $\langle t \rangle$ done by the researchers.^[79,84,85,115] For FeS₂, the AFM image shown in Figure 3A is of the largest size fraction. As it can be observed, the length of the platelets varied from 400 to 200 nm. Whereas for β-boron, the length of the platelet shown in the image is ≈6 μm. For B₄C, the length of the platelets varies from 500 to 100 nm, and for Ge-platelets $L \approx 12.5 \mu\text{m}$. One point to note here is that while FeS₂ is the only anisotropic compound among all these 4 examples, it is the one with the smallest nanosheet length.

Figure 3B shows the variation of $\langle \alpha \rangle$ versus $\langle t \rangle$ only for the materials for which a reasonably large (>50) data set has been analyzed as listed in Table 1. Each different data point represents a different publication and the compounds are divided as anisotropic (represented by triangular symbols) and isotropic (represented by circular symbols). As shown in Figure 3B, $\alpha > 1$ for all the materials, indicating a non-0D (and non-3D) nature. For the anisotropic material, FeS₂, $\langle \alpha \rangle \approx 4$, is consistent with the lower end of the aspect-ratio-scale for layered materials. This low aspect ratio is expected due to

small but non-zero bonding anisotropy in FeS₂ compared to layered materials. What is unexpected is that FeS₂ has the lowest aspect ratio in this study with several platelets exfoliated from isotropic NL-NvdW materials displaying a higher aspect ratio.

Although the isotropic compound B₄C also displayed a low aspect-ratio, $\langle \alpha \rangle \approx 4$, several papers described platelets derived from isotropic materials with higher values of $\langle \alpha \rangle$. For example, nanoplatelets of Ge displayed high aspect ratio values of $\langle \alpha \rangle \approx 80$. For context, this value is higher than that for LPE graphene which tends to display aspect ratios of ≈50.^[49]

Another example is β-boron as shown in Figure 3. Although it has been exfoliated by many research groups,^[86–90,112,115–118] unfortunately only two papers^[86,115] have counted a reasonably large number of platelets and did the statistical analysis to estimate the aspect-ratio as shown in Figure 3B. Li et al.^[86] exfoliated β-B in two different solvents, DMF and IPA by probe sonication, and all other parameters were kept constant in the experiment (see Table 1), but estimated $\langle \alpha \rangle$ of the platelets obtained by using DMF solvent is significantly large ($\langle \alpha \rangle = 77$) as compared to the platelets obtained by using IPA solvent ($\langle \alpha \rangle = 9$) as shown in Figure 3B. Zhang et al.^[115] has used solvothermal treated β-B as a starting material in LPE to accomplish exfoliation by probe sonication in acetone. As it can be seen in Figure 3B, this has resulted in a very high aspect-ratio of 1440. The platelets however have well-defined edges, as shown in the AFM image of β-B in Figure 3A. This

unexpected high aspect-ratio can be attributed to the introduction of solvothermal process prior to the probe sonication.

We have also observed that a few other research groups^[68,75] have reported the statistical analysis by AFM, without giving the number of platelets counted. Examples include papers describing LPE by bath sonication in DMF solvent of naturally existing minerals such as hematite ($\alpha\text{-Fe}_2\text{O}_3$),^[68] goethite ($\alpha\text{-FeO(OH)}$),^[75] and calcite (CaCO_3).^[75] The estimated $\langle\alpha\rangle$ is significantly higher ($\alpha_{\text{hematite}} \approx 3000$, $\alpha_{\text{CaCO}_3} \approx 1000$, $\alpha_{\text{FeO(OH)}} \approx 470$). However, without knowing the sample size, one cannot have confidence in the accuracy of the statistical analysis. As such we have not included this data in Figure 3B.

The reports described above of high-aspect-ratio platelets produced by LPE of low-anisotropy starting materials are both surprising and puzzling. While these reports may be suggestive of previously unidentified exfoliation mechanisms, we must also face the possibility that some of the AFM reported in the literature is not accurate. While AFM has been used for some time to determine the thickness of the 2D-platelets, care has to be taken in analyzing the data. Even for 2D nanosheets exfoliated from layered materials (which have very distinct shapes characterized by sharp edges and well-defined steps and terraces) analysis of AFM images can be extremely challenging. As mentioned above, this can be due to solvent residues and impurities or due to commonly observed scanning artifacts that can often be mistaken as nanosheets.^[138] For nanoplatelets produced by LPE of NL-NvdW materials, this is even more of an issue due to the less well-defined morphology.

We emphasize that it is extremely important to accurately measure the aspect ratio of liquid exfoliated nanosheets, particularly those prepared from nonlayered and especially isotropic nonlayered materials. If high aspect-ratio platelets can be produced by LPE of low-anisotropy materials, then this could mean that the models of exfoliation expressed previously^[32,49] are incorrect. Alternatively, it could be evidence of some additional factors, for example, crack formation during cryo-treatments or some sort of flow effects during LPE, which favor the formation of quasi-2D particles. Either way, definitive aspect-ratio measurements are critically important, as they could lead to new mechanistic insights. However, given the pitfalls associated with AFM listed above, we believe that AFM measurements alone cannot be relied upon when reporting surprising results such as high platelet aspect ratios. In these situations, corroborating evidence, such as the correlation of the L -distribution with that measured by TEM or by correlating images with those obtained from scanning Raman spectroscopy, are absolutely essential.

Finally, it is worth considering if all of the nanoplatelets produced by LPE of NL-NvdW materials can actually be considered as 2D. There are a number of factors to consider. A commonly used definition of 2D (or quasi-2D) materials is that they are thin enough that confinement effects result in physical properties that differ from the bulk. This is unlikely to be the case for those nanoplatelets that have thicknesses of order tens of nanometers. However, even thicker objects can be “quasi-2D-like” if their aspect ratio is large enough to yield a platelet-like geometry. This is why we use the broad term “nanoplatelets”. However, it is clear from Figure 3B that exfoliation of some NL-NvdW materials (i.e., FeS_2 , B_4C) yields nano-objects with

thickness >10 nm and aspect ratios as low as 4. It is reasonable to ask whether such objects can be referred to as quasi-2D objects or even nanoplatelets or whether they are in fact nanoparticles. To the authors knowledge there is no agreed criterion as to the borderline between a particle and a platelet. One might set an arbitrary aspect ratio above which objects are platelets. However, this will be subjective—what does one consider a platelet? Is an iPhone ($\alpha \approx 20$) platelet-like? Or a textbook (Atkins, “Physics Chemistry” has $\alpha \approx 7$)? We suggest platelets are those objects with aspect ratio above 5–10. However, it will be necessary for the community to come to some consensus on this issue.

3.4. Cleavage Behavior and Basal Plane

In crystalline materials, cleavage is defined as a fracture along a definite plane in the lattice structure, which results in an atomically smooth surface.^[139] It is quantified by the cleavage energy which is closely related to the surface energy.^[140] In layered materials, cleavage parallel to the atomic layers is the most favorable due to the low energy required to break the weak interlayer forces. The lower the cleavage energy, the thinner we expect the platelets to be. Alternatively, the strong in-plane chemical bonds require a lot of energy to fracture during exfoliation. Therefore, the stronger the in-plane bonds are, the larger we expect the lateral dimensions of the nanosheets to be (large nanosheets require less chemical bonds to be broken to create edges).^[49,50] In other words, for higher anisotropy between the in-plane and out-of-plane bond strength, we expect an increased nanosheet aspect ratio.^[49,50]

Since layered materials have high anisotropy, cleavage predominately occurs parallel to the basal plane direction.^[32] However, if a layered material with strong in-plane-bonding has out-of-plane bonding via forces (e.g., electrostatic in the case of metal borides^[141]) which are stronger than vdW forces, then the cleavage energy is increased and the mechanical anisotropy is reduced. Such materials are relatively more difficult to cleave, leading to thicker platelets with a lower aspect ratio.^[141] Importantly, in the case of NL-NvdW crystals, bonding is strong in all three directions meaning there is no plane which is very easily cleaved. So, for cleavage to happen, rupturing of chemical bonds must take place. Then, by analogy with nanoparticles, we would imagine the probability of cleavage along a given atomic plane during exfoliation to be smaller for planes with larger cleavage or surface energies. This is the basis of the Wulff construction used to determine the equilibrium shape of nanoparticles.^[142] Because of this, a number of papers^[143,144] have used theoretical approaches to identify crystals with low-cleavage-energy planes with the idea that such materials might be candidates for exfoliation. For example, Friedrich et al. studied nonlayered binary and ternary metal oxides and found considerable variation in cleavage energy with some materials containing planes with cleavage energy approaching that of graphite. In cases where exfoliation leads to platelets, we expect the large area facets to consist of atomic planes with low cleavage or surface energy while the edge facets should consist of atomic planes with high cleavage or surface energy. In line with the model of Backes et al.,^[49] the platelet aspect ratio should be roughly proportional to

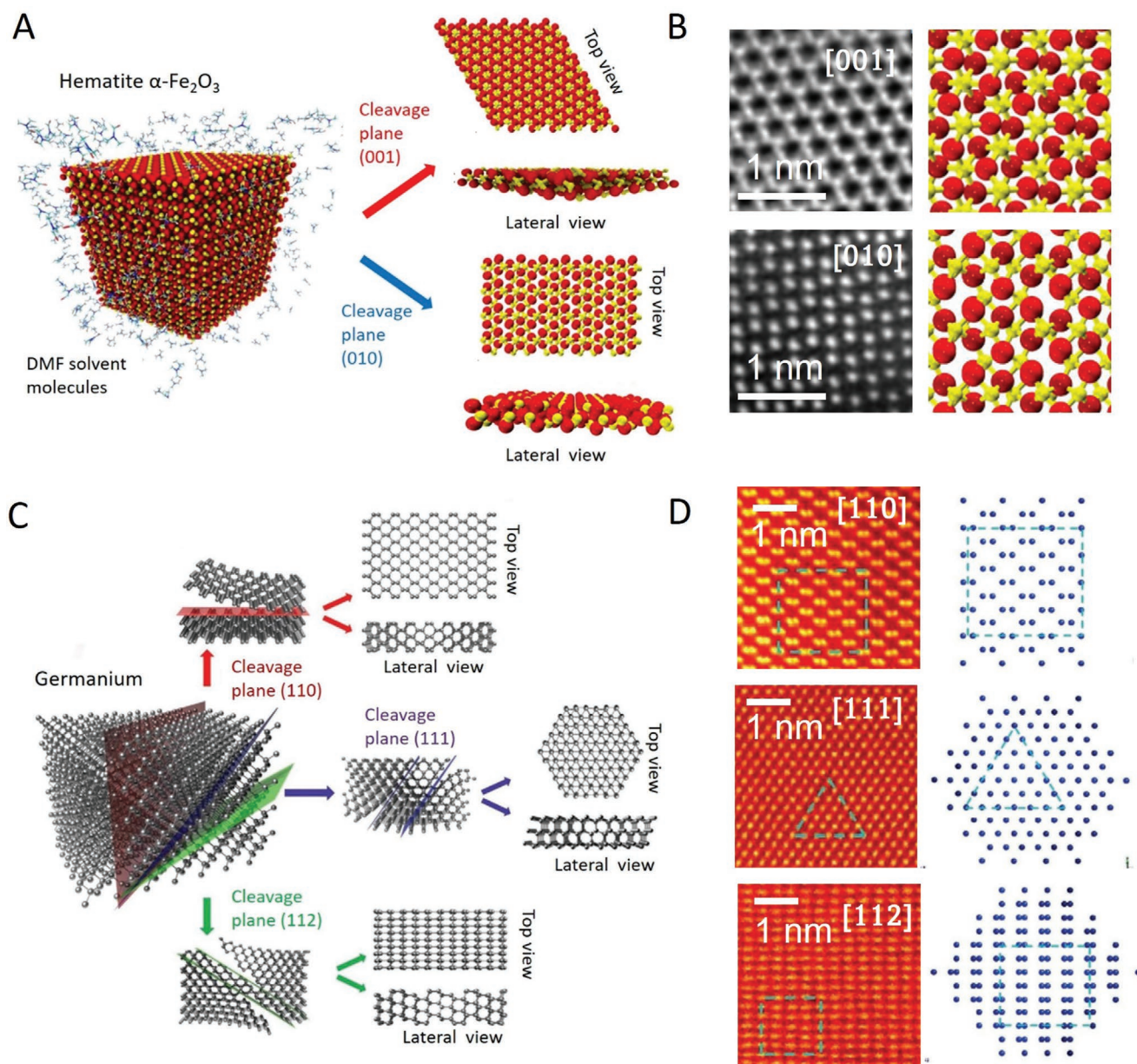


Figure 4. Examples of the possible cleavage planes in bulk NL-NvdW crystals. A) Bulk crystal structure of hematite crystal ($\alpha\text{-Fe}_2\text{O}_3$) and its two possible crystallographic cleavage planes (001) and (010). The lateral and top view of the monolayers obtained by these two possible cleavage planes is also shown. The red and yellow color represent the O and Fe atoms respectively. B) STEM images from LPE produced hematene platelets showed basal plane in [001], and [010] orientation (left column) and molecular dynamic simulated planar view of the [001] and [010] orientation (right column). A,B) Reproduced with permission.^[68] Copyright 2018, The Authors, published by Springer Nature. C) Crystal structure of $\alpha\text{-Ge}$, and its three possible crystallographic cleavage planes (110), (111), and (112). The top and lateral view of the monolayer obtained from each possible cleavage plane is also shown. D) STEM images obtained from the nanosheet of Ge (left column), and models of the respective crystallographic planes (right column). C,D) Reproduced with permission.^[84] Copyright 2021, Wiley-VCH.

the ratio of the (higher) edge facet surface energy to the (lower) large area facet surface energy.

However, it is worth noting that this picture is somewhat complicated by the effects of structural relaxation of the platelet surfaces after exfoliation. Using computational studies on a range of materials extracted from databases, Friedrich et al.^[144] showed that the details of the surface reconstruction coupled with the oxidation states of the ions on the nanosheet surfaces

determine the overall cost of exfoliation. Critically, for 2D-platelets exfoliated from NL-NvdW crystals, this energy cost appears to differ from that predicted solely from surface or cleavage energies. This means that the most preferable cleavage direction may not be that associated with the lowest surface energy when the cleavage results in a very thin nanosheet.

Balan et al.^[68] demonstrated exfoliation of bulk hematite into 2D-hematene platelets (Figure 4A).^[68] Experimentally,

using STEM imaging on a single atomic layer of hematene, the authors observed two basal planes, (001) and (010) as shown in Figure 4B. The atomic arrangement of atoms in the STEM images matches well with the molecular dynamic simulated atomic structure of the orientation as shown in Figure 4B.^[68] However, these results are based on a single hematene nanosheet. It is impossible to rule out the possibility that there may be other nanoplatelets in the dispersion which may have different basal planes. However, this data does show that

Materials	Solvents										
	N,N-Dimethyl formamide	2-Propanol	N-methyl-2-pyrrolidone	Water	Ethanol	Acetone	N,N-dimethylacetamide	Methanol	2-Butanol	Benzyl benzoate	Ethylene glycol
α -Fe ₂ O ₃	●										
FeTiO ₃	●										
FeCr ₂ O ₄	●										
MnTe	●										
β -Boron	●	●	●	●		●			●	●	●
α -Boron	●										
α -FeO(OH)	●										
CaCO ₃	●										
PbS	●										
FeS ₂	●		●								
TiC	●		●								
WC	●										
Si	●	◐	●	◐	●				●		
B ₄ C	●	●	●			●	●				
Ti		●									
Ge	◐			◐							
Mg					●						
Sn					●						
SiC	◐			◐							
LiMn ₂ O ₄					●						
LiFePO ₄					●						
LaB ₆				●							

Figure 5. List of solvents used in the LPE of different NL-NvdW compounds. The solvents are arranged in the order of the most to least used (left to right). Black solid circles are used as a symbol to represent the solvent used in LPE, whereas the fractional volume percentages of the solvent are represented with incomplete solid circles. For example, for SiC, a 1:1 mixture of 2-propanol: water was used as a liquid media to achieve LPE. Tungsten oxide (α -WO₃) is not included in the list of materials as it was exfoliated in aqueous solution of acidic bovine serum albumin.^[64]

cleavage along (001) and (010) planes is possible, consistent with them being relatively low surface energy planes.

Another example is the Ge crystal shown in Figure 4C. Gibaja et al.^[84] has used density functional theory (DFT) to simulate the surface energies of the miller indices (100), (110), (111), and (112). The results showed that the reconstructed (100) surface plane is the lowest in energy with a small difference over the reconstructed (110) surface, and unreconstructed (111) and (112) surface.^[84] Therefore, they predict that there are three possible basal planes in 2D-Ge as shown in Figure 3C.^[84] Experimentally, using STEM imaging, they have observed three basal planes of nanoplatelets of Ge, (111), (110), and (112) as shown in Figure 4D, consistent with the idea that cleavage preferentially occurs along low surface energy planes.^[84] The authors also mentioned (110) is the most common basal plane, however, the size of the sample set is not given.^[84]

Guo et al.^[85] showed the presence of six different basal planes (300), (1200), (0150), (060), (411), and (221) in nanoplatelets obtained by the exfoliation of isotropic B₄C. The authors also mentioned a sample size of over 30 flakes has been analyzed by HRTEM imaging. However, the statistical analysis on this data set is not given. Their density functional theory (DFT) simulations did not show a significant difference in the values of binding energies of different orientations, indicated that many planes are energetically favorable.

Furthermore, Yadav et al.^[70] showed 2D-chromiteen nanoplatelets produced by LPE of chromite possess multiple basal planes (111), (222), and (533). Similarly, Liu et al.^[75] demonstrated the presence of more than one basal plane in different nanoplatelets, such as for α -FeO(OH): (001) and (111), for PbS: (001) and (111), and for CaCO₃: (104), (1014), (1010), (1120) and (1011). Also, Wang et al.^[78] demonstrated that LPE produced silicon nanoplatelets have (111) orientation.

We believe basal plane analysis by imaging a single, or fewer nanoplatelets by using HRTEM, or STEM techniques can be misleading as it may represent only a minority subpopulation and shows only what is possible not what is probable. We believe a thorough statistical analysis using reasonably large sample sets to obtain a good estimate of the most dominant basal plane is the best approach, although we accept it is a challenging and time-consuming approach.

3.5. Solvents and Surface Passivation

One of the most common types of LPE of layered materials involves sonication in a stabilizing solvent.^[5,6,16,26,41,46,145] Good solvents are usually distinguished by their surface energy, although Hildebrand, and Hansen solubility parameters, are also used.^[6,101,146,147] For layered materials, an ideal solvent is one whose surface energy is matched to that of the basal plane of the exfoliated nanosheet.^[6,43,100] Such matching is thought to minimize the exfoliation energy.^[6,101,146,147]

For layered materials, we tend to focus on the vdW interaction of the solvent molecules with the basal plane of the nanosheet rather than any interaction of solvents with the nanosheet edge.^[147] This is simply because the large aspect ratio of most layered material nanosheets means the edges can effectively be ignored. However, it is worth noting that,

for nanosheets produced from exfoliation of layered materials, while the basal plane is chemically inert owing to its vdW structure, chemically active dangling bonds are present at the edges due to the breaking of covalent bonds during the exfoliation process. It has been shown that during exfoliation directly in a solvent in ambient conditions, the reactive dangling bonds at edges undergo passivation via oxidation by the redox-active species produced by the sonolysis of the solvent.^[32,92,148]

This passivation is very important in the LPE of NL-NvdW materials because such materials have no inert basal plane. On exfoliation of NL-NvdW compounds the entire surface (i.e., both large area and edge facets) of the as-produced nanoplatelets consists of dangling bonds and so is chemically active and will be passivated. The chemical nature of the groups which passivate the surface of nanoplatelets plays a crucial role in determining the stability of the suspension because they will determine the nature of the interfacial interaction with the solvent.

Thus, the question of what an ideal solvent for LPE of NL-NvdW compounds is probably closely related to the details of the reaction of the solvent with the unpassivated platelet surface and subsequent interaction with the passivated platelet surface. Here we will discuss what solvents have been used to date in the exfoliation of NL-NvdW materials.

Figure 5 shows a list of all the solvents corresponding to different materials used by researchers to achieve successful LPE. The solvents are arranged in the order of most to least used. As observed in Figure 5, *N,N*-dimethylformamide (DMF) is the most common solvent used by the researchers. The crystals exfoliated by this solvent were α -Fe₂O₃,^[68] FeTiO₃,^[69] FeCr₂O₄,^[70] MnTe,^[71] β -B,^[86,112,118] α -B,^[114] α -FeO(OH),^[75] CaCO₃,^[75] PbS,^[75] FeS₂,^[82] TiC,^[113] WC,^[113] Si,^[73,78] and B₄C.^[85] In fact, if we correlate this result with Figure 1B, DMF has been mostly used in bath sonication LPE process for α -Fe₂O₃,^[68] FeTiO₃,^[69] FeCr₂O₄,^[70] MnTe,^[71] β -B,^[112] α -B,^[114] α -FeO(OH),^[75] CaCO₃,^[75] PbS,^[75] FeS₂,^[82] TiC,^[113] and WC.^[113]

Sonolysis of solvents due to the chemical effects of ultrasound has been studied in the past. The violent collapse of acoustic cavitation bubbles during bath sonication produces high temperature, pressure, and shear rates locally, resulting in sonolysis of the solvent and the production of radicals.^[32,92,148,149] These radicals, which originate from the solvent itself, may play a significant role in the passivation of the platelet surface.

For LPE produced platelets from NL-NvdW materials, we believe prolonged bath sonication with DMF as a liquid medium in ambient probably have resulted in the passivation of the surface by oxygen (–O) or hydroxide (–OH) radicals which aids in exfoliation. Other solvents have also been used by authors as shown in Figure 5 such as 2-propanol (IPA), IPA/water mixture, *N*-methyl-2-pyrrolidone (NMP), ethanol, etc. All these solvents contain water molecules and dissolved oxygen which can probably surface oxidize the dangling bonds of nanoplatelets.

As shown by us,^[79] LPE produced nanoplatelets of FeS₂ in NMP were surface passivated by the oxides, hydroxides, and the ketone group of NMP residues as confirmed by Fourier transform infrared spectroscopy (FT-IR) measurements. Wang et al.^[78] has also shown the existence of Si–OH and Si–O in the exfoliated nanoplatelets of silicon produced by LPE in various solvents by FT-IR measurements. Even the 2D-platelets

of boron produced by the Zhang group in IPA solvent by a combination of probe and bath sonication showed the presence of stretching vibrations corresponding to –OH, B–O, B–H, C=O, and B–O–B in FT-IR spectroscopy measurements.^[89] Gibaja et al.^[84] has also confirmed the presence of Ge–O and Ge–H functional groups on the surface of LPE produced Ge platelets.

NL-NvdW nanosheets likely display rich surface chemistry because the presence of multiple sonication-induced radicals leads to a range of functional groups passivating the surface. Because these groups originate from the solvent itself, they are of course compatible with the solvent leading to a strong platelet-solvent interfacial interaction which aids in stabilizing the dispersions. Thus, the ideal solvent is probably one that readily passivates the surface of as-produced nanoplatelets. However, more detailed studies in this regard are required to be sure of the role of solvent in the LPE process.

As described in ref. [79] quantitative information on the functional group density energy can be achieved by performing energy-dispersive X-ray spectroscopy (EDX) in the TEM on a platelet by platelet basis. This means using EDX to measure elemental compositions on a number (usually >30) of individual flakes, while simultaneously measuring the flake dimensions. In the first instance, this technique gives statistical platelet stoichiometry data which allows the researcher to confirm the composition of the exfoliated materials. However, it can also be used to confirm that elements (such as oxygen) associated with the functional groups that are present on the platelet surface and even to estimate the surface density. As described in ref. [79] for FeS₂ platelets, the surface is oxidized by groups containing O atoms. EDX was then used to measure the atomic ratio, O/Fe, as a function of platelet size, *L*. A simple model was used to predict that if the oxygen atoms were associated with the platelet surface, then O/Fe \propto 1/*L* consistent with the experimental data. Fitting this equation to the O/Fe versus *L* gave an estimate of the functional group density which turned out to be similar to the expected dangling bond density.

Above, we have discussed the passivation of dangling-bond-rich surfaces by reaction with solvent molecules. To date this process has been uncontrolled and unintentional and has presumably been determined by combination of the solvent used, the nature of the surface to be passivated and the exfoliation conditions. However, one could envisage controlling the reaction between the freshly cleaved surface and the supporting liquid to yield predetermined functional groups leading to an activated interface. This might be achieved by adding reactive species to the solvent during exfoliation which are intended to react with newly created dangling bonds on the surface. The resultant functional groups could be designed to influence the surface properties of the nanoplatelet. This might allow one to control parameters such as the adsorption characteristics, catalytic activity, or electrical properties (via doping) of the nanomaterial. Such in-situ surface activation could become a very powerful tool to enhance the properties of nanoplatelets.

3.6. Exfoliation Yield

LPE of layered compounds generally results in relatively high yields due to the ease with which weak forces can be broken.

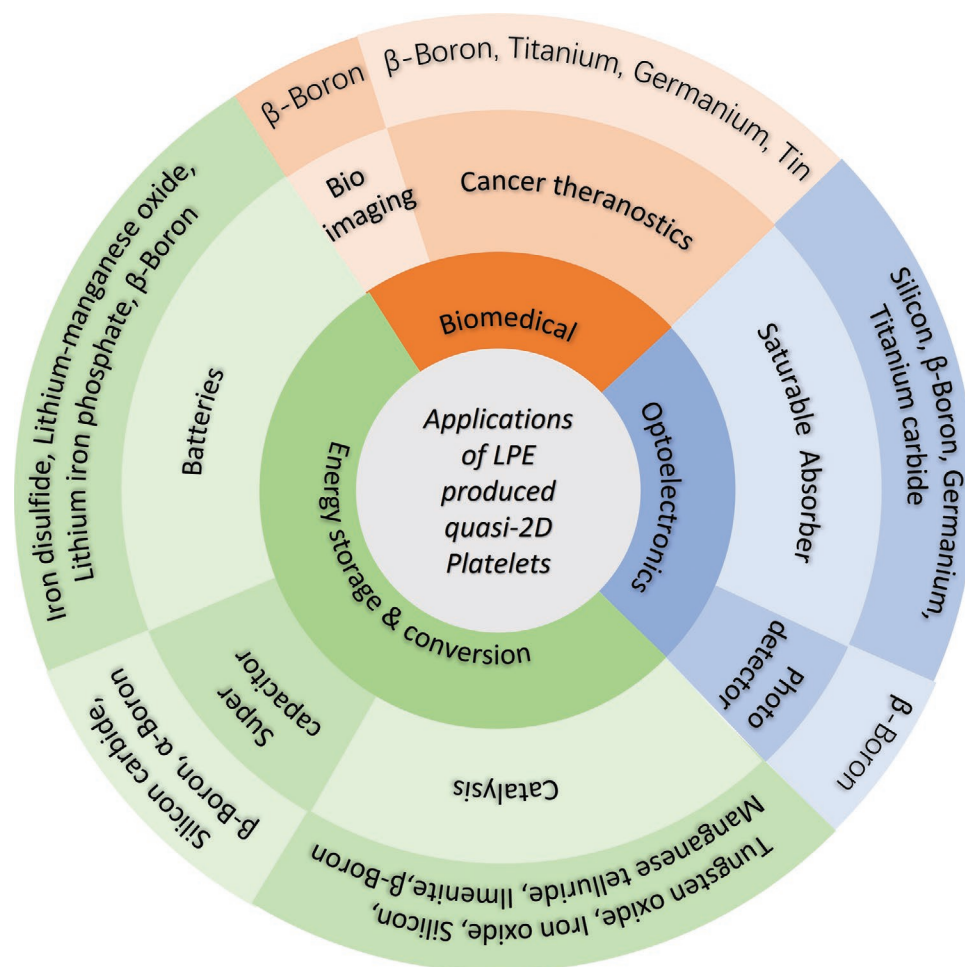


Figure 6. A detailed chart showing the demonstrated applications of LPE produced nanoplatelets of different NL-NvdW materials. See Table S3, Supporting Information, for references to all the materials shown here.

The Ferrari group has showed the yield of graphene and nano-graphite reached 100% under high shear rate 10^8 s^{-1} by using microfluidic processor.^[98] However, in case of NL-NvdW compounds, we intuitively expect the yield to be lower as the exfoliation demands high-energy to break the strong bonds. Nevertheless, it is important to measure this parameter in order to scale up the production rate from technological applicability. Unfortunately, we found very few papers which have reported the exfoliation yield. As reported by us,^[79] the yield for the production of FeS_2 nanoplatelets in NMP solvent by probe sonication was 3–3.5%. Similar range $\approx 4\%$ was also reported by Wang et al.^[118] in the production of β -B platelets by probe sonication in 2-butanol. But surprisingly Lin et al.^[116] achieved a reasonable high yield of 20% for β -B platelets by probe sonication in NMP solvent but the LPE was performed at very low temperature of -20 to $-25 \text{ }^\circ\text{C}$.^[116] A similar yield of $\approx 20\%$ was also reported by Fan et al.^[88] for β -B platelets in benzyl-benzoate solvent by bath sonication. Although the data set is small, these examples indeed shows that the yield varies between different solvents, as well as, between different types of LPE. In the short term, yield can be improved by the recycling of unexfoliated sediment material.^[36] However, in the long term, improvements in yield will require a better understanding of the exfoliation mechanism. We note that LPE experimental details on

all NL-NvdW compounds considered in this review are given in Table S2, Supporting Information.

4. Applications of Nanoplatelets

LPE-produced nanoplatelet inks offer a wide spectrum of applications in different fields such as energy storage and conversion (e.g., batteries, supercapacitors, catalysis, etc.), optoelectronics (e.g., saturable absorbers, photodetector, etc.) and in biomedical applications (e.g., bioimaging and cancer theranostics) as shown in **Figure 6**. Depending upon the area of application, distinct properties offered by these novel nanoplatelets are preferred. Here we had briefly discussed selected examples from the literature in each field on how these nanoplatelets are favorable for each respective application (see Table S3, Supporting Information, for references to all the materials given in **Figure 6**).

4.1. Energy Storage and Conversion

The 2D-geometry of nonlayered nanoplatelets offers significant advantages over its 3D-lattices as these nanoplatelets can display large structural distortions, possess high density of surface

dangling bonds and unsaturated surface atoms. These makes them perfect candidates in catalysis due to their high surface chemical activity.^[67] Therefore, nanoplatelets of Si,^[78] β -B,^[88] α -WO₃,^[64] α -Fe₂O₃,^[68] MnTe,^[71] and FeTiO₃^[69] had shown good catalytic performance as demonstrated by several researchers.

Also, due to the ultrathin nature of the nanoplatelets, they offer fast interfacial charge transfer resulting in lower recombination rates and enhanced carrier mobility, making them good candidates in photo and electrocatalysis. As shown by Wang et al.^[78] LPE-produced silicon nanoplatelets etched with hydrofluoric acid showed photocatalytic hydrogen productivity at the rate of 220 $\mu\text{mol h}^{-1} \text{g}^{-1}$.^[78] Further, Ajayan group demonstrated that composites of LPE produced nanoplatelets of MnTe,^[71] FeTiO₃,^[69] and α -Fe₂O₃,^[68] mixed with titania nanotubes showed photoelectrochemical water splitting under visible light.

In addition, these nanoplatelets show better electrochemical and rate performance due to short solid state diffusion time for ions which is very important for Li-ion batteries. Therefore, LPE produced nanoplatelets of numerous compounds has shown impressive results as active electrodes materials for high-performance lithium-ion batteries.^[65,79,81,116] For example, Tai et al.^[65] have shown the rate-performance and cyclic stability in LiMn₂O₄ and LiFePO₄ was improved significantly when nanoplatelets were used instead of bulk 3D-material, due to reduced solid-state diffusion lengths.^[65] We have also shown that the Li-storing anodes fabricated from nanoplatelets of FeS₂ mixed with carbon nanotubes display near-theoretical capacities of $\approx 1000 \text{ mAh g}^{-1}$.^[79,81] Lin et al.^[116] have used LPE-produced β -B nanoplatelets as polysulfide immobilizers and electrocatalyst in Li-S batteries, achieving high stability and very good rate-performance, reporting a specific capacity of 721 mAh g⁻¹ at high charge/discharge current.^[116]

Furthermore, owing to their high-specific surface area, conductivity, and good thermal and chemical stability, NL-NvdW nanoplatelets have also shown potential as supercapacitor electrode materials.^[76,86,114] For example, the electrochemical performance of α -B platelets mixed with PANI showed a specific capacitance of 960 F g⁻¹ with capacitive retention of 95% after 1000 cycles.^[114] Li et al.^[86] used LPE-produced nanoplatelets of β -B to produce supercapacitor electrodes combining outstanding energy density of 46.1 Wh kg⁻¹ with a power density of 478.5 W kg⁻¹, as well as excellent cyclic stability.^[86]

4.2. Optoelectronics

LPE-produced NL-NvdW nanoplatelets have been shown to display interesting nonlinear optical properties with researchers demonstrating applications as saturable absorbers and photodetectors due to their ultrafast carrier response, and broadband absorption in the nanoplatelets. For example, Ma et al.^[117] showed that LPE-produced nanoplatelets of β -B had excellent broadband nonlinear optical properties in ultrafast laser photonics.^[117] The β -B platelets served as an optical switch due to their saturable absorber properties and produced ultra-short pulses with duration <700 fs in the near to mid-infrared for ultrafast mode-locking applications.^[117] The Zhang group^[113] has shown that the nanoplatelets of TiC are excellent saturable absorbers and have large modulation depths and low saturation

intensities across the infrared.^[113] Zhou et al.^[91] has shown LPE-produced platelets of Ge have excellent broadband nonlinear optical properties. All these examples indeed demonstrate that new materials could have significant potential in photonic technologies.^[73,91,113,117]

Moreover, LPE-produced nanoplatelets of β -B have also shown excellent optoelectronic performance as a self-powered photodetector due to its semiconducting bandgap.^[150] The as-synthesized nanoplatelets were used in photoelectrochemical (PEC) and field-effect transistor (FET) type photodetectors.^[150] The PEC device photoresponsivity was as high as 92 $\mu\text{A W}^{-1}$ in the UV region, whereas the FET device showed a tunable photoresponsivity of 175–280 $\mu\text{A W}^{-1}$ for 405 nm irradiation.^[150]

4.3. Biomedical

Nanoplatelets of some nonlayered compounds such as β -B,^[87,89,90] Ti,^[72] Ge,^[77] and Sn^[83] possess good biocompatibility and offer low cytotoxicity,^[72,77,83,87,89,90] which makes them interesting candidates in the field of biomedical applications in areas such as in bioimaging and in cancer theranostics.^[72,77,83,87,89,90] For example, Ma et al.^[89] demonstrated that the LPE-produced β -B platelets showed blue fluorescence with a quantum yield of 10.6% which is used to successfully image the cervical cancer cell line HeLa and hepatocarcinoma cell line Huh-7.^[89] Due to the planar geometry of the nanoplatelets, it offers high drug-loading capacity which is favorable for application in cancer chemotherapy. Further, the ultrathin thickness of these biocompatible nanoplatelets enables them to respond to external stimuli such as pH and light. Thus, these nanoplatelets are of great interest for various optical therapies such as photothermal therapy and photodynamic therapy. For example, Williams et al.^[90] developed a multifunctional nanoplatform based on LPE-produced β -B nanoplatelets, for synergistic chemotherapy and low-temperature photothermal therapy.^[90] The researchers demonstrated that β -B platelets functionalized with peptide cRGD, co-carrying the chemotherapeutic drug doxorubicin, and the heat shock protein inhibitor 17AAG, responds well to acidic pH and NIR laser irradiation to release the drug and kill cancer cells, and inhibit tumor growth at low temperatures.^[90] These examples demonstrate that LPE-produced 2D-nanoplatelets of biocompatible materials have the potential in advancing the field of oncology.^[72,77,83,87,89,90]

5. Summary and Outlook

Here, we have reviewed the growing field of liquid-phase exfoliation of nonlayered compounds. After first summarizing the LPE of layered compounds, we surveyed recent developments in LPE of nonlayered compounds. We examined different aspects of this field including the lattice structure of exfoliable non-layered materials and the details of the cleavage plane as well as characterization of the resultant platelets. We discussed the solvents used and the surface passivation of the nanosheets and finally examined the potential applications of such materials. We have tried to correlate results across different materials to bring a deeper understanding of the topic.

In layered materials, there has been significant experimental work on LPE over the last decade leading to rapid progress. By comparison, research on the LPE of nonlayered materials is still in its infancy. Nevertheless, it is already clear that this area shows great promise and will lead to a multitude of new 2D-nanoplatelets with interesting and useful properties. However, there are a number of challenges to be addressed as well as significant questions that remain to be answered before this field can flourish.

Perhaps most important will be to develop an understanding of the mechanism for the exfoliation of nonlayered materials. For some anisotropic nonlayered materials such as FeS₂, it appears as if the exfoliation mechanism is similar to that which applies to layered materials. However, the exfoliation of isotropic materials such as silicon cannot be understood within this framework. It will be crucial to identify whether one broad overarching mechanism is at work or do different mechanisms apply for different materials? In addition, it will be important to determine if the exfoliation mechanism is predominantly limited by intrinsic factors such as cleavage energies or extrinsic factors such as cryo-induced crack formation or flow phenomena which might favor the exfoliation of platelets over particles. Such mechanistic understanding will enable advances in other areas as indicated below.

Insights into exfoliation mechanisms should cast light on the particularly puzzling question of why isotropic materials such as silicon can be exfoliated by LPE to yield platelets. This is very unexpected as the cleavage energies of all atomic planes in silicon crystals lie within a relatively narrow range. Considerations associated with the Wulff construction would lead one to expect isotropic silicon to form particles rather than platelets under liquid exfoliation.^[15] That platelets have been produced by multiple research teams implies that a more complicated exfoliation mechanism is at work. Equally surprising is the fact that isotropic materials such as germanium and boron not only produce nanoplatelets under exfoliation but yield platelets that can be very thin and have aspect ratios of up to 1000. These are degrees of thinness and aspect ratio that are not found for liquid exfoliated layered materials. Importantly, mechanistic understanding may yield insights into the factors limiting aspect ratio allowing us to control platelet dimensions in a way that has been hitherto impossible.

Mechanistic understanding should help us to answer another important question: what criteria determine which nonlayered compounds can undergo exfoliation and which cannot? Initially, the answer to this question may have seemed obvious: anisotropic bonding schemes facilitate exfoliation in the same way as occurs for layered materials. However, the demonstration that isotropic materials could be exfoliated into high aspect ratio platelets showed us that we do not understand this topic well enough to answer this question.

In addition to answering these questions, there are a multitude of other challenges which must be addressed. The most basic is to improve the efficiency of the exfoliation process both in terms of yield, production rate and energy cost. In addition, it would be interesting to control the cleavage behavior such that we were no longer limited to low surface energy basal planes to the point where we could specify the nature of the basal surface. Furthermore, it will be important to gain control

of the passivation of the newly cleaved surfaces to allow us to control the surface activity of the nanoplatelets and adapt their properties toward new applications. The ability to produce new materials, fine tune the surface chemistry and dimensions of the nanoplatelets will open up a host of new applications that have not previously been possible.

Despite the breadth of questions to be answered and problems to be solved, we predict that this research area will continue to grow, driven by the promise of a wide range of new 2D materials, displaying a host of exciting properties. Given the substantial success and broad versatility of LPE as applied to layered materials, we believe the ability to exfoliate nonlayered materials will significantly broaden the scope and range of (quasi)-2D materials that can be mass-produced via this facile and versatile top-down process. Although it has generated as many questions as answers, this recent progression of LPE from layered to nonlayered is very exciting and has ignited a new research direction that is worthy of deep exploration.

Supporting Information

Supporting Information is available from the Wiley Online Library or from the author.

Acknowledgements

The authors acknowledge the European Research Council Advanced Grant (FUTURE-PRINT), the European Union under Graphene Flagship cores 2 & 3 (grant agreements 785219 and 881603). They have also received support from the Science Foundation Ireland (SFI) funded centre AMBER (SFI/12/RC/2278) and availed of the facilities of the SFI-funded AML and ARM labs. They also thank Claudia Backes, Bharathi Konkana, Ahin Roy, and Kevin Synnatschke for valuable discussions.

Open access funding provided by IReL.

Conflict of Interest

The authors declare no conflict of interest.

Keywords

anisotropic materials, isotropic materials, liquid-phase exfoliation, nanoplatelets, nonlayered materials

Received: March 8, 2022

Revised: April 7, 2022

Published online:

- [1] K. S. Novoselov, D. Jiang, F. Schedin, T. J. Booth, V. V. Khotkevich, S. V. Morozov, A. K. Geim, *Proc. Natl. Acad. Sci. USA* **2005**, *102*, 10451.
- [2] P. Miró, M. Audiffred, T. Heine, *Chem. Soc. Rev.* **2014**, *43*, 6537.
- [3] M. Xu, T. Liang, M. Shi, H. Chen, *Chem. Rev.* **2013**, *113*, 3766.
- [4] F. Bonaccorso, A. Bartolotta, J. N. Coleman, C. Backes, *Adv. Mater.* **2016**, *28*, 6136.
- [5] V. Nicolosi, M. Chhowalla, M. G. Kanatzidis, M. S. Strano, J. N. Coleman, *Science* **2013**, *340*, 1226419.

- [6] J. N. Coleman, M. Lotya, A. O'Neill, S. D. Bergin, P. J. King, U. Khan, K. Young, A. Gaucher, S. De, R. J. Smith, *Science* **2011**, *331*, 568.
- [7] K. S. Novoselov, A. K. Geim, S. V. Morozov, D.-e. Jiang, Y. Zhang, S. V. Dubonos, I. V. Grigorieva, A. A. Firsov, *Science* **2004**, *306*, 666.
- [8] a) D. Akinwande, C. J. Brennan, J. S. Bunch, P. Egberts, J. R. Felts, H. Gao, R. Huang, J.-S. Kim, T. Li, Y. Li, *Extreme Mech. Lett.* **2017**, *13*, 42; b) A. Gupta, T. Sakthivel, S. Seal, *Prog. Mater. Sci.* **2015**, *73*, 44; c) X. Li, L. Tao, Z. Chen, H. Fang, X. Li, X. Wang, J.-B. Xu, H. Zhu, *Appl. Phys. Rev.* **2017**, *4*, 021306.
- [9] a) X. Liu, M. C. Hersam, *Nat. Rev. Mater.* **2019**, *4*, 669; b) Q. Ma, G. Ren, K. Xu, J. Z. Ou, *Adv. Opt. Mater.* **2021**, *9*, 1056; c) S. Wang, D. W. Zhang, P. Zhou, *Sci. Bull.* **2019**, *64*, 1056; d) O. A. Moses, L. Gao, H. Zhao, Z. Wang, M. L. Adam, Z. Sun, K. Liu, J. Wang, Y. Lu, Z. Yin, X. Yu, *Mater. Today* **2021**, *50*, 116; e) N. R. Glavin, R. Rao, V. Varshney, E. Bianco, A. Apte, A. Roy, E. Ringe, P. M. Ajayan, *Adv. Mater.* **2020**, *32*, 1904302.
- [10] a) Á. Coogan, Y. K. Gun'ko, *Mater. Adv.* **2021**, *2*, 146; b) R. Dong, T. Zhang, X. Feng, *Chem. Rev.* **2018**, *118*, 6189.
- [11] J. Yu, J. Li, W. Zhang, H. Chang, *Chem. Sci.* **2015**, *6*, 6705.
- [12] Z. Cai, B. Liu, X. Zou, H.-M. Cheng, *Chem. Rev.* **2018**, *118*, 6091.
- [13] a) Z. Yang, Z. Wu, Y. Lyu, J. Hao, *InfoMat* **2019**, *1*, 98; b) M. M. Juvaid, M. S. R. Rao, *Mater. Today: Proc.* **2021**, *35*, 494; c) J. D. Yao, Z. Q. Zheng, G. W. Yang, *Prog. Mater. Sci.* **2019**, *106*, 100573.
- [14] L. A. Walsh, C. L. Hinkle, *Appl. Mater. Today* **2017**, *9*, 504.
- [15] J. N. Coleman, *Adv. Funct. Mater.* **2009**, *19*, 3680.
- [16] C. Huo, Z. Yan, X. Song, H. Zeng, *Sci. Bull.* **2015**, *60*, 1994.
- [17] X. Cai, Y. Luo, B. Liu, H.-M. Cheng, *Chem. Soc. Rev.* **2018**, *47*, 6224.
- [18] X. Guo, Z. Wang, W. Zhu, H. Yang, *RSC Adv.* **2017**, *7*, 9009.
- [19] a) A. J. Mannix, B. Kiraly, M. C. Hersam, N. P. Guisinger, *Nat. Rev. Chem.* **2017**, *1*, 0014; b) F. Wang, Z. Wang, Q. Wang, F. Wang, L. Yin, K. Xu, Y. Huang, J. He, *Nanotechnology* **2015**, *26*, 292001.
- [20] S. Das, M. Kim, J.-w. Lee, W. Choi, *Crit. Rev. Solid State Mater. Sci.* **2014**, *39*, 231.
- [21] D. H. Lee, Y. Sim, J. Wang, S.-Y. Kwon, *APL Mater.* **2020**, *8*, 030901.
- [22] A. O'Neill, U. Khan, J. N. Coleman, *Chem. Mater.* **2012**, *24*, 2414.
- [23] J. N. Coleman, *Acc. Chem. Res.* **2013**, *46*, 14.
- [24] E. Varrla, K. R. Paton, C. Backes, A. Harvey, R. J. Smith, J. McCauley, J. N. Coleman, *Nanoscale* **2014**, *6*, 11810.
- [25] E. Varrla, C. Backes, K. R. Paton, A. Harvey, Z. Gholamvand, J. McCauley, J. N. Coleman, *Chem. Mater.* **2015**, *27*, 1129.
- [26] L. Niu, J. N. Coleman, H. Zhang, H. Shin, M. Chhowalla, Z. Zheng, *Small* **2016**, *12*, 272.
- [27] J. Shen, Y. He, J. Wu, C. Gao, K. Keyshar, X. Zhang, Y. Yang, M. Ye, R. Vajtai, J. Lou, *Nano Lett.* **2015**, *15*, 5449.
- [28] R. Narayan, S. O. Kim, *Nano Convergence* **2015**, *2*, 20.
- [29] a) D. Pacile, J. C. Meyer, Ç. Girit, A. Zettl, *Appl. Phys. Lett.* **2008**, *92*, 133107; b) A. Splendiani, L. Sun, Y. Zhang, T. Li, J. Kim, C.-Y. Chim, G. Galli, F. Wang, *Nano Lett.* **2010**, *10*, 1271; c) Z. Yin, H. Li, H. Li, L. Jiang, Y. Shi, Y. Sun, G. Lu, Q. Zhang, X. Chen, H. Zhang, *ACS Nano* **2012**, *6*, 74; d) J. Brivio, D. T. L. Alexander, A. Kis, *Nano Lett.* **2011**, *11*, 5148; e) H. Li, Q. Zhang, C. C. R. Yap, B. K. Tay, T. H. T. Edwin, A. Olivier, D. Baillargeat, *Adv. Funct. Mater.* **2012**, *22*, 1385; f) W. Zhao, Z. Ghorannevis, L. Chu, M. Toh, C. Kloc, P.-H. Tan, G. Eda, *ACS Nano* **2013**, *7*, 791; g) G. Plechinger, P. Nagler, J. Kraus, N. Paradiso, C. Strunk, C. Schüller, T. Korn, *Phys. Status Solidi RRL* **2015**, *9*, 457; h) H. Li, G. Lu, Y. Wang, Z. Yin, C. Cong, Q. He, L. Wang, F. Ding, T. Yu, H. Zhang, *Small* **2013**, *9*, 1974; i) S. P. Koenig, R. A. Doganov, H. Schmidt, A. H. Castro Neto, B. Özyilmaz, *Appl. Phys. Lett.* **2014**, *104*, 103106; j) A. Castellanos-Gomez, L. Vicarelli, E. Prada, J. O. Island, K. L. Narasimha-Acharya, S. I. Blanter, D. J. Groenendijk, M. Buscema, G. A. Steele, J. V. Alvarez, *2D Mater.* **2014**, *1*, 025001; k) A. Castellanos-Gomez, *J. Phys. Chem. Lett.* **2015**, *6*, 4280.
- [30] a) E. Gao, S.-Z. Lin, Z. Qin, M. J. Buehler, X.-Q. Feng, Z. Xu, *J. Mech. Phys. Solids* **2018**, *115*, 248; b) L. Yuan, J. Ge, X. Peng, Q. Zhang, Z. Wu, Y. Jian, X. Xiong, H. Yin, J. Han, *AIP Adv.* **2016**, *6*, 125201; c) Y. Huang, Y.-H. Pan, R. Yang, L.-H. Bao, L. Meng, H.-L. Luo, Y.-Q. Cai, G.-D. Liu, W.-J. Zhao, Z. Zhou, L.-M. Wu, Z.-L. Zhu, M. Huang, L.-W. Liu, L. Liu, P. Cheng, K.-H. Wu, S.-B. Tian, C.-Z. Gu, Y.-G. Shi, Y.-F. Guo, Z. G. Cheng, J.-P. Hu, L. Zhao, G.-H. Yang, E. Sutter, P. Sutter, Y.-L. Wang, W. Ji, X.-J. Zhou, et al., *Nat. Commun.* **2020**, *11*, 2453; d) M. Yi, Z. Shen, *J. Mater. Chem. A* **2015**, *3*, 11700.
- [31] C. Zhang, J. Tan, Y. Pan, X. Cai, X. Zou, H.-M. Cheng, B. Liu, *Nat. Sci. Rev.* **2019**, *7*, 324.
- [32] Z. Li, R. J. Young, C. Backes, W. Zhao, X. Zhang, A. A. Zhukov, E. Tillotson, A. P. Conlan, F. Ding, S. J. Haigh, *ACS Nano* **2020**, *14*, 10976.
- [33] A. Ciesielski, P. Samori, *Chem. Soc. Rev.* **2014**, *43*, 381.
- [34] Q. Yan, W. Dai, J. Gao, X. Tan, L. Lv, J. Ying, X. Lu, J. Lu, Y. Yao, Q. Wei, R. Sun, J. Yu, N. Jiang, D. Chen, C.-P. Wong, R. Xiang, S. Maruyama, C.-T. Lin, *ACS Nano* **2021**, *15*, 6489.
- [35] W. Zhao, M. Fang, F. Wu, H. Wu, L. Wang, G. Chen, *J. Mater. Chem.* **2010**, *20*, 5817.
- [36] K. R. Paton, E. Varrla, C. Backes, R. J. Smith, U. Khan, A. O'Neill, C. Boland, M. Lotya, O. M. Istrate, P. King, *Nat. Mater.* **2014**, *13*, 624.
- [37] Y.-Z. Wang, T. Chen, X.-F. Gao, H.-H. Liu, X.-X. Zhang, *Mater. Express* **2017**, *7*, 491.
- [38] J. Shang, F. Xue, C. Fan, E. Ding, *Mater. Lett.* **2016**, *181*, 144.
- [39] S. Bellani, E. Petroni, A. E. Del Rio Castillo, N. Curreli, B. Martín-García, R. Oropesa-Nuñez, M. Prato, F. Bonaccorso, *Adv. Funct. Mater.* **2019**, *29*, 1807659.
- [40] A. E. D. R. Castillo, V. Pellegrini, A. Ansaldo, F. Ricciardella, H. Sun, L. Marasco, J. Buha, Z. Dang, L. Gagliani, E. Lago, *Mater. Horiz.* **2018**, *5*, 890.
- [41] a) J. B. Boland, A. Harvey, R. Tian, D. Hanlon, V. Vega-Mayoral, B. Szydłowska, A. Griffin, T. Stimpel-Lindner, S. Jaskaniec, V. Nicolosi, *Nanoscale Adv.* **2019**, *1*, 1560; b) A. Harvey, X. He, I. J. Godwin, C. Backes, D. McAteer, N. C. Berner, N. McEvoy, A. Ferguson, A. Shmeliov, M. E. G. Lyons, *J. Mater. Chem. A* **2016**, *4*, 11046; c) P. Yasaei, B. Kumar, T. Foroozan, C. Wang, M. Asadi, D. Tuschel, J. E. Indacochea, R. F. Klie, A. Salehi-Khojin, *Adv. Mater.* **2015**, *27*, 1887; d) D. Hanlon, C. Backes, E. Doherty, C. S. Cucinotta, N. C. Berner, C. Boland, K. Lee, A. Harvey, P. Lynch, Z. Gholamvand, *Nat. Commun.* **2015**, *6*, 8563.
- [42] a) J. B. Boland, R. Tian, A. Harvey, V. Vega-Mayoral, A. Griffin, D. V. Horvath, C. Gabbett, M. Breshears, J. Pepper, Y. Li, *2D Mater.* **2020**, *7*, 035015; b) R. Tian, A. Griffin, M. McCrystall, M. Breshears, A. Harvey, C. Gabbett, D. V. Horvath, C. Backes, Y. Jing, T. Heine, *Adv. Energy Mater.* **2021**, *11*, 2002364.
- [43] Y. Hernandez, V. Nicolosi, M. Lotya, F. M. Blighe, Z. Sun, S. De, I. T. McGovern, B. Holland, M. Byrne, Y. K. Gun'ko, *Nat. Nanotechnol.* **2008**, *3*, 563.
- [44] a) M. Yi, Z. Shen, S. Ma, X. Zhang, *J. Nanopart. Res.* **2012**, *14*, 1003; b) M. Bat-Erdene, M. Batmunkh, C. J. Shearer, S. A. Tawfik, M. J. Ford, L. Yu, A. J. Sibley, A. D. Slattery, J. S. Quinton, C. T. Gibson, *Small Methods* **2017**, *1*, 1700260; c) J. Kang, J. D. Wood, S. A. Wells, J.-H. Lee, X. Liu, K.-S. Chen, M. C. Hersam, *ACS Nano* **2015**, *9*, 3596; d) V. Sresht, A. A. H. Padua, D. Blankschtein, *ACS Nano* **2015**, *9*, 8255; e) M. Lee, A. K. Roy, S. Jo, Y. Choi, A. Chae, B. Kim, S. Y. Park, I. In, *Nanotechnology* **2017**, *28*, 125603; f) E. P. Nguyen, B. J. Carey, T. Daeneke, J. Z. Ou, K. Latham, S. Zhuikov, K. Kalantar-zadeh, *Chem. Mater.* **2015**, *27*, 53.
- [45] S. Lin, Y. Chui, Y. Li, S. P. Lau, *FlatChem* **2017**, *2*, 15.
- [46] Y. Liu, X. He, D. Hanlon, A. Harvey, J. N. Coleman, Y. Li, *ACS Nano* **2016**, *10*, 8821.
- [47] M. Kajbafvala, M. Farbod, *J. Colloid Interface Sci.* **2018**, *527*, 159.

- [48] C. Backes, T. M. Higgins, A. Kelly, C. Boland, A. Harvey, D. Hanlon, J. N. Coleman, *Chem. Mater.* **2017**, *29*, 243.
- [49] C. Backes, D. Campi, B. M. Szydłowska, K. Synnatschke, E. Ojala, F. Rashvand, A. Harvey, A. Griffin, Z. Sofer, N. Marzari, *ACS Nano* **2019**, *13*, 7050.
- [50] L.-J. Ji, Y. Qin, D. Gui, W. Li, Y. Li, X. Li, P. Lu, *Chem. Mater.* **2018**, *30*, 8732.
- [51] a) Y. Nalawade, J. Pepper, A. Harvey, A. Griffin, D. Caffrey, A. G. Kelly, J. N. Coleman, *ACS Appl. Electron. Mater.* **2020**, *2*, 3233; b) S. Conti, L. Pimpolari, G. Calabrese, R. Worsley, S. Majee, D. K. Polyushkin, M. Paur, S. Pace, D. H. Keum, F. Fabbri, *Nat. Commun.* **2020**, *11*, 3566; c) S. Chung, K. Cho, T. Lee, *Adv. Sci.* **2019**, *6*, 1801445; d) A. G. Kelly, D. O'Suilleabhain, C. Gabbett, J. N. Coleman, *Nat. Rev. Mater.* **2021**, *7*, 217; e) A. G. Kelly, T. Hallam, C. Backes, A. Harvey, A. S. Esmaily, I. Godwin, J. Coelho, V. Nicolosi, J. Lauth, A. Kulkarni, *Science* **2017**, *356*, 69; f) N. Curreli, M. Serri, D. Spirito, E. Lago, E. Petroni, B. Martín-García, A. Politano, B. Gürbulak, S. Duman, R. Krahne, *Adv. Funct. Mater.* **2020**, *30*, 1908427.
- [52] a) S. K. Lee, D. Chu, J. Yoo, E. K. Kim, *Sol. Energy Mater. Sol. Cells* **2018**, *184*, 9; b) V. Bianchi, T. Carey, L. Viti, L. Li, E. H. Linfield, A. G. Davies, A. Tredicucci, D. Yoon, P. G. Karagiannidis, L. Lombardi, *Nat. Commun.* **2017**, *8*, 15763; c) D. Dodoo-Arhin, R. C. T. Howe, G. Hu, Y. Zhang, P. Hiralal, A. Bello, G. Amaratunga, T. Hasan, *Carbon* **2016**, *105*, 33; d) K.-S. Chen, I. Balla, N. S. Luu, M. C. Hersam, *ACS Energy Lett.* **2017**, *2*, 2026.
- [53] G. Patel, V. Pillai, M. Vora, *J. Nanosci. Nanotechnol.* **2019**, *19*, 5054.
- [54] C. S. Boland, U. Khan, G. Ryan, S. Barwich, R. Charifou, A. Harvey, C. Backes, Z. Li, M. S. Ferreira, M. E. Möbius, *Science* **2016**, *354*, 1257.
- [55] a) B. Yang, Y. Chen, J. Shi, *Chem* **2018**, *4*, 1284; b) H. Zhang, T. Fan, W. Chen, Y. Li, B. Wang, *Bioact. Mater.* **2020**, *5*, 1071.
- [56] M. Naguib, M. Kurtoglu, V. Presser, J. Lu, J. Niu, M. Heon, L. Hultman, Y. Gogotsi, M. W. Barsoum, *Adv. Mater.* **2011**, *23*, 4248.
- [57] M. Naguib, V. N. Mochalin, M. W. Barsoum, Y. Gogotsi, *Adv. Mater.* **2014**, *26*, 992.
- [58] a) M. Mariano, O. Mashtalir, F. Q. Antonio, W.-H. Ryu, B. Deng, F. Xia, Y. Gogotsi, A. D. Taylor, *Nanoscale* **2016**, *8*, 16371; b) K. Maleski, C. E. Ren, M.-Q. Zhao, B. Anasori, Y. Gogotsi, *ACS Appl. Mater. Interfaces* **2018**, *10*, 24491.
- [59] Y. Gogotsi, B. Anasori, *ACS Nano* **2019**, *13*, 8491.
- [60] M. Naguib, M. W. Barsoum, Y. Gogotsi, *Adv. Mater.* **2021**, *33*, 2103393.
- [61] a) M. Radovic, M. W. Barsoum, *Am. Ceram. Soc. Bull.* **2013**, *92*, 20; b) M. Magnuson, M. Mattesini, *Thin Solid Films* **2017**, *621*, 108.
- [62] J.-C. Lei, X. Zhang, Z. Zhou, *Front. Phys.* **2015**, *10*, 276.
- [63] M. Magnuson, J. Halim, L.-Å. Näslund, *J. Electron Spectrosc. Relat. Phenom.* **2018**, *224*, 27.
- [64] G. Guan, J. Xia, S. Liu, Y. Cheng, S. Bai, S. Y. Tee, Y. W. Zhang, M. Y. Han, *Adv. Mater.* **2017**, *29*, 1700326.
- [65] Z. Tai, C. M. Subramaniyam, S. L. Chou, L. Chen, H. K. Liu, S. X. Dou, *Adv. Mater.* **2017**, *29*, 1700605.
- [66] a) Y. Dou, L. Zhang, X. Xu, Z. Sun, T. Liao, S. X. Dou, *Chem. Soc. Rev.* **2017**, *46*, 7338; b) P. Tao, S. Yao, F. Liu, B. Wang, F. Huang, M. Wang, *J. Mater. Chem. A* **2019**, *7*, 23512.
- [67] Y. Wang, Z. Zhang, Y. Mao, X. Wang, *Energy Environ. Sci.* **2020**, *13*, 3993.
- [68] A. P. Balan, S. Radhakrishnan, C. F. Woellner, S. K. Sinha, L. Deng, C. de Los Reyes, B. M. Rao, M. Paulose, R. Neupane, A. Apte, *Nat. Nanotechnol.* **2018**, *13*, 602.
- [69] A. Puthirath Balan, S. Radhakrishnan, R. Kumar, R. Neupane, S. K. Sinha, L. Deng, C. A. de los Reyes, A. Apte, B. M. Rao, M. Paulose, *Chem. Mater.* **2018**, *30*, 5923.
- [70] T. P. Yadav, S. N. Shirodkar, N. Lertcumfu, S. Radhakrishnan, F. N. Sayed, K. D. Malviya, G. Costin, R. Vajtai, B. I. Yakobson, C. S. Tiwary, P. M. Ajayan, *Adv. Mater. Interfaces* **2018**, *5*, 1800549.
- [71] A. Puthirath Balan, S. Radhakrishnan, R. Neupane, S. Yazdi, L. Deng, C. A. de los Reyes, A. Apte, A. B. Puthirath, B. M. Rao, M. Paulose, *ACS Appl. Nano Mater.* **2018**, *1*, 6427.
- [72] Z. Xie, S. Chen, Y. Duo, Y. Zhu, T. Fan, Q. Zou, M. Qu, Z. Lin, J. Zhao, Y. Li, *ACS Appl. Mater. Interfaces* **2019**, *11*, 22129.
- [73] M. Wang, F. Zhang, Z. Wang, X. Xu, *Materials* **2019**, *12*, 201.
- [74] C. Zhang, Y. Xu, P. Lu, C. Wei, C. Zhu, H. Yao, F. Xu, J. Shi, *Angew. Chem., Int. Ed.* **2019**, *58*, 8814.
- [75] S. Liu, L. Xie, H. Qian, G. Liu, H. Zhong, H. Zeng, *J. Mater. Chem. A* **2019**, *7*, 15411.
- [76] Q. Chen, Y. Jiang, Y. Wang, H. Li, C. Yu, J. Cui, Y. Qin, J. Sun, J. Yan, H. Zheng, *Inorg. Chem. Commun.* **2019**, *106*, 174.
- [77] C. Feng, J. Ouyang, Z. Tang, N. Kong, Y. Liu, L. Fu, X. Ji, T. Xie, O. C. Farokhzad, W. Tao, *Matter* **2020**, *3*, 127.
- [78] Y. Wang, R. Cai, J. Zhang, J. Cui, Y. Qin, Y. Zhang, J. Wu, K. Chatterjee, P. M. Ajayan, Y. Wu, *J. Phys. Chem. Lett.* **2020**, *11*, 8668.
- [79] H. Kaur, R. Tian, A. Roy, M. McCrystal, D. V. Horvath, G. Lozano Onrubia, R. Smith, M. Ruether, A. Griffin, C. Backes, *ACS Nano* **2020**, *14*, 13418.
- [80] S. K. John, A. A. Anappara, *RSC Adv.* **2020**, *10*, 31788.
- [81] H. Kaur, R. Tian, A. Roy, M. McCrystal, R. Smith, D. V. Horvath, V. Nicolosi, J. N. Coleman, *FlatChem* **2021**, *30*, 100295.
- [82] A. B. Puthirath, A. P. Balan, E. F. Oliveira, V. Sreepal, F. C. Robles Hernandez, G. Gao, N. Chakingal, L. M. Sassi, P. Thibeorchews, G. Costin, *J. Phys. Chem. C* **2021**, *125*, 18927.
- [83] J. Ouyang, L. Zhang, L. Li, W. Chen, Z. Tang, X. Ji, C. Feng, N. Tao, N. Kong, T. Chen, Y.-N. Liu, W. Tao, *Nano-Micro Lett.* **2021**, *13*, 90.
- [84] C. Gibaja, D. Rodríguez-San-Miguel, W. S. Paz, I. Torres, E. Salagre, P. Segovia, E. G. Michel, M. Assebban, P. Ares, D. Hernández-Maldonado, *Adv. Mater.* **2021**, *33*, 2006826.
- [85] Y. Guo, A. Gupta, M. S. Gilliam, A. Debnath, A. Yousaf, S. Saha, M. D. Levin, A. A. Green, A. K. Singh, Q. H. Wang, *Nanoscale* **2021**, *13*, 1652.
- [86] H. Li, L. Jing, W. Liu, J. Lin, R. Y. Tay, S. H. Tsang, E. H. T. Teo, *ACS Nano* **2018**, *12*, 1262.
- [87] X. Ji, N. Kong, J. Wang, W. Li, Y. Xiao, S. T. Gan, Y. Zhang, Y. Li, X. Song, Q. Xiong, *Adv. Mater.* **2018**, *30*, 1803031.
- [88] Q. Fan, C. Choi, C. Yan, Y. Liu, J. Qiu, S. Hong, Y. Jung, Z. Sun, *Chem. Commun.* **2019**, *55*, 4246.
- [89] D. Ma, J. Zhao, J. Xie, F. Zhang, R. Wang, L. Wu, W. Liang, D. Li, Y. Ge, J. Li, *Nanoscale Horiz.* **2020**, *5*, 705.
- [90] Z. Fu, G. R. Williams, S. Niu, J. Wu, F. Gao, X. Zhang, Y. Yang, Y. Li, L.-M. Zhu, *Nanoscale* **2020**, *12*, 14739.
- [91] L. Zhou, Y. Wang, Y. Wang, S. Xiao, J. He, *Opt. Express* **2021**, *29*, 39115.
- [92] A. Jawaid, D. Nepal, K. Park, M. Jespersen, A. Qualley, P. Mirau, L. F. Drummy, R. A. Vaia, *Chem. Mater.* **2016**, *28*, 337.
- [93] K. Kouroupis-Agalou, A. Liscio, E. Treossi, L. Ortolani, V. Morandi, N. M. Pugno, V. Palermo, *Nanoscale* **2014**, *6*, 5926.
- [94] a) Y. Xu, H. Cao, Y. Xue, B. Li, W. Cai, *Nanomaterials* **2018**, *8*, 942; b) L. Li, M. Zhou, L. Jin, L. Liu, Y. Mo, X. Li, Z. Mo, Z. Liu, S. You, H. Zhu, *Front. Mater.* **2019**, *6*, 325.
- [95] Y. Liu, C. Liang, J. Wu, S. J. Varma, Y. Nakanishi, A. Aliyan, A. A. Martf, Y. Wang, B. Xie, J. Kumar, K. Layne, N. Chopra, I. Odeh, R. Vajtai, J. Thomas, X. Peng, W. Yang, P. M. Ajayan, *Mater. Today* **2019**, *22*, 17.
- [96] a) D. Voiry, J. Yang, J. Kupferberg, R. Fullon, C. Lee, H. Y. Jeong, H. S. Shin, M. Chhowalla, *Science* **2016**, *353*, 1413; b) F. Lei, M. Yang, F. Jiang, H. Zhang, Z. Zhang, D. Z. Sun, *Chem. Eng. J.* **2019**, *360*, 673.
- [97] E. B. Flint, K. S. Suslick, *Science* **1991**, *253*, 1397.

- [98] P. G. Karagiannidis, S. A. Hodge, L. Lombardi, F. Tomarchio, N. Decorde, S. Milana, I. Goykhman, Y. Su, S. V. Mesite, D. N. Johnstone, *ACS Nano* **2017**, *11*, 2742.
- [99] a) H. Wang, W. Lv, J. Shi, H. Wang, D. Wang, L. Jin, J. Chao, P. A. van Aken, R. Chen, W. Huang, *ACS Sustainable Chem. Eng.* **2019**, *8*, 84; b) X. Zhang, J. Deng, J. Yan, Y. Song, Z. Mo, J. Qian, X. Wu, S. Yuan, H. Li, H. Xu, *Appl. Surf. Sci.* **2019**, *490*, 117; c) Y. Wang, Y. Liu, J. Zhang, J. Wu, H. Xu, X. Wen, X. Zhang, C. S. Tiwary, W. Yang, R. Vajtai, *Sci. Adv.* **2017**, *3*, e1701500.
- [100] Y. Hernandez, M. Lotya, D. Rickard, S. D. Bergin, J. N. Coleman, *Langmuir* **2010**, *26*, 3208.
- [101] K. G. Zhou, N. N. Mao, H. X. Wang, Y. Peng, H. L. Zhang, *Angew. Chem.* **2011**, *123*, 11031.
- [102] J. Li, F. Ye, S. Vaziri, M. Muhammed, M. C. Lemme, M. Östling, *Adv. Mater.* **2013**, *25*, 3985.
- [103] S. Ravula, S. N. Baker, G. Kamath, G. A. Baker, *Nanoscale* **2015**, *7*, 4338.
- [104] J. Shen, J. Wu, M. Wang, P. Dong, J. Xu, X. Li, X. Zhang, J. Yuan, X. Wang, M. Ye, *Small* **2016**, *12*, 2741.
- [105] a) A. Abun, B.-R. Huang, A. Saravanan, D. Kathiravan, P.-D. Hong, *J. Alloys Compd.* **2020**, *832*, 155005; b) C.-X. Hu, Y. Shin, O. Read, C. Casiraghi, *Nanoscale* **2021**, *13*, 460.
- [106] M. Lotya, Y. Hernandez, P. J. King, R. J. Smith, V. Nicolosi, L. S. Karlsson, F. M. Blighe, S. De, Z. Wang, I. T. McGovern, *J. Am. Chem. Soc.* **2009**, *131*, 3611.
- [107] P. May, U. Khan, J. M. Hughes, J. N. Coleman, *J. Phys. Chem. C* **2012**, *116*, 11393.
- [108] R. J. Smith, P. J. King, M. Lotya, C. Wirtz, U. Khan, S. De, A. O'Neill, G. S. Duesberg, J. C. Grunlan, G. Moriarty, *Adv. Mater.* **2011**, *23*, 3944.
- [109] L. Vitos, A. V. Ruban, H. L. Skriver, J. Kollár, *Surf. Sci.* **1998**, *411*, 186.
- [110] R. Tran, Z. Xu, B. Radhakrishnan, D. Winston, W. Sun, K. A. Persson, S. P. Ong, *Sci. Data* **2016**, *3*, 160080.
- [111] Z.-y. Gao, S. U. N. Wei, Y.-h. Hu, *Trans. Nonferrous Met. Soc. China* **2014**, *24*, 2930.
- [112] P. Ranjan, T. K. Sahu, R. Bhushan, S. S. Yamijala, D. J. Late, P. Kumar, A. Vinu, *Adv. Mater.* **2019**, *31*, 1900353.
- [113] C.-X. Hu, Z. Tian, Q. Xiao, Z.-T. Zhu, X.-Y. Li, G.-H. Dun, H.-R. Wu, Y.-L. Tang, Q. Wang, H.-L. Zhang, *Small Struct.* **2021**, *2*, 2100039.
- [114] S. Göktuna, N. Taşaltın, *Phys. E* **2021**, *134*, 114833.
- [115] F. Zhang, L. She, C. Jia, X. He, Q. Li, J. Sun, Z. Lei, Z.-H. Liu, *RSC Adv.* **2020**, *10*, 27532.
- [116] H. Lin, H. Shi, Z. Wang, Y. Mu, S. Li, J. Zhao, J. Guo, B. Yang, Z.-S. Wu, F. Liu, *ACS Nano* **2021**, *15*, 17327.
- [117] C. Ma, P. Yin, K. Khan, A. K. Tareen, R. Huang, J. Du, Y. Zhang, Z. Shi, R. Cao, S. Wei, *Small* **2021**, *17*, 2006891.
- [118] X. Wang, J. Liang, Q. You, J. Zhu, F. Fang, Y. Xiang, J. Song, *Angew. Chem.* **2020**, *132*, 23765.
- [119] a) R. S. Vemuri, M. H. Engelhard, C. V. Ramana, *ACS Appl. Mater. Interfaces* **2012**, *4*, 1371; b) M. B. Johansson, P. T. Kristiansen, L. Duda, G. A. Niklasson, L. Österlund, *J. Phys.: Condens. Matter* **2016**, *28*, 475802.
- [120] a) J. Nouri, T. Khoshravesh, S. Khanahmadzadeh, A. Salehabadi, M. Enhessari, *Int. J. Nano Dimens.* **2016**, *7*, 15; b) S. Douafer, H. Lahmar, M. Benamira, G. Rekhila, M. Trari, *J. Phys. Chem. Solids* **2018**, *118*, 62.
- [121] T. Ogitsu, E. Schwegler, G. Galli, *Chem. Rev.* **2013**, *113*, 3425.
- [122] G. Liu, L. C. Yin, P. Niu, W. Jiao, H. M. Cheng, *Angew. Chem., Int. Ed.* **2013**, *52*, 6242.
- [123] R. H. Misho, W. A. Murad, *Sol. Energy Mater. Sol. Cells* **1992**, *27*, 335.
- [124] J. A. Cerón, D. A. Téllez, J. Roa-Rojas, *J. Electron. Mater.* **2022**, *51*, 822.
- [125] A. T. Raghavender, N. H. Hong, K. J. Lee, M.-H. Jung, Z. Skoko, M. Vasilevskiy, M. F. Cerqueira, A. P. Samantilleke, *J. Magn. Magn. Mater.* **2013**, *331*, 129.
- [126] S. Chatterjee, U. Pal, *Opt. Eng.* **1993**, *32*, 2923.
- [127] H. Zhang, M. Bayne, S. Fernando, B. Legg, M. Zhu, R. L. Penn, J. F. Banfield, *J. Phys. Chem. C* **2011**, *115*, 17704.
- [128] V. Domnich, S. Reynaud, R. A. Haber, M. Chhowalla, *J. Am. Ceram. Soc.* **2011**, *94*, 3605.
- [129] H. G. Grimmeiss, *Semiconductors* **1999**, *33*, 939.
- [130] A. Münster, K. Sagel, G. Schlamp, *Nature* **1954**, *174*, 1154.
- [131] A. Pawbake, R. Waykar, A. Jadhavar, R. Kulkarni, V. Waman, A. Date, D. Late, H. Pathan, S. Jadhkar, *Mater. Lett.* **2016**, *183*, 315.
- [132] J. Phillips, *Bonds and Bands in Semiconductors*, Elsevier, Amsterdam, The Netherlands **2012**.
- [133] M. Chen, *NPG Asia Mater.* **2011**, *3*, 82.
- [134] C. Fan, J. Li, L. Wang, *Sci. Rep.* **2014**, *4*, 6993.
- [135] Z. Gholamvand, D. McAteer, A. Harvey, C. Backes, J. N. Coleman, *Chem. Mater.* **2016**, *28*, 2641.
- [136] C. Backes, R. J. Smith, N. McEvoy, N. C. Berner, D. McCloskey, H. C. Nerl, A. O'Neill, P. J. King, T. Higgins, D. Hanlon, N. Scheuschner, J. Maultzsch, L. Houben, G. S. Duesberg, J. F. Donegan, V. Nicolosi, J. N. Coleman, *Nat. Commun.* **2014**, *5*, 4576.
- [137] C. Backes, B. M. Szydłowska, A. Harvey, S. Yuan, V. Vega-Mayoral, B. R. Davies, P.-I. Zhao, D. Hanlon, E. J. G. Santos, M. I. Katsnelson, *ACS Nano* **2016**, *10*, 1589.
- [138] P. Eaton, K. Batziou, in *Atomic Force Microscopy: Methods and Protocols*, Vol. 1886 (Eds: N. C. Santos, F. A. Carvalho), Humana Press, New York, USA **2019**, p. 3.
- [139] U. Vaknin, D. Sherman, S. Gorfman, *IUCr* **2021**, *8*, 793.
- [140] Y. Hirsh, S. Gorfman, D. Sherman, *Acta Mater.* **2020**, *193*, 338.
- [141] A. Yousaf, M. S. Gilliam, S. L. Y. Chang, M. Augustin, Y. Guo, F. Tahir, M. Wang, A. Schwindt, X. S. Chu, D. O. Li, *J. Phys. Chem. C* **2021**, *125*, 6787.
- [142] R. F. Strickland-Constable, *Kinetics and Mechanism of Crystallization*, Academic Press, London, UK **1968**.
- [143] N. Mounet, M. Gibertini, P. Schwaller, D. Campi, A. Merkys, A. Marrazzo, T. Sohier, I. E. Castelli, A. Cepellotti, G. Pizzi, N. Marzari, *Nat. Nanotechnol.* **2018**, *13*, 246.
- [144] R. Friedrich, M. Ghorbani-Asl, S. Curtarolo, A. V. Krashenninnikov, *Nano Lett.* **2022**, *22*, 989; *arXiv: 2110.01366*, **2021**.
- [145] a) H. Kaur, S. Yadav, A. K. Srivastava, N. Singh, S. Rath, J. J. Schneider, O. P. Sinha, R. Srivastava, *Nano Res.* **2018**, *11*, 343; b) H. Kaur, S. Yadav, A. K. Srivastava, N. Singh, J. J. Schneider, O. P. Sinha, V. V. Agrawal, R. Srivastava, *Sci. Rep.* **2016**, *6*, 34095.
- [146] U. Halim, C. R. Zheng, Y. Chen, Z. Lin, S. Jiang, R. Cheng, Y. Huang, X. Duan, *Nat. Commun.* **2013**, *4*, 2213.
- [147] J. M. Hughes, D. Aherne, J. N. Coleman, *J. Appl. Polym. Sci.* **2013**, *127*, 4483.
- [148] L. Muscuso, S. Cravanzola, F. Cesano, D. Scarano, A. Zecchina, *J. Phys. Chem. C* **2015**, *119*, 3791.
- [149] V. Misik, L. J. Kirschenbaum, P. Riesz, *J. Phys. Chem.* **1995**, *99*, 5970.
- [150] D. Ma, R. Wang, J. Zhao, Q. Chen, L. Wu, D. Li, L. Su, X. Jiang, Z. Luo, Y. Ge, *Nanoscale* **2020**, *12*, 5313.
- [151] B. Peng, F. Cheng, Z. Tao, J. Chen, *J. Chem. Phys.* **2010**, *133*, 034701.



Harnet Kaur is currently a Postdoctoral Fellow in Graphene Flagship project at the CRANN research institute, Trinity College Dublin. After receiving her Bachelors, and Master's Degree in physics from University of Delhi, she started her Ph.D. at the National Physical Laboratory in 2014. She received her Ph.D. degree in 2018, and then joined Trinity College Dublin in the year 2019 as a postdoc in Jonathan Coleman's group. Her research interests focuses on the design and synthesis of novel 2D materials for applications in energy storage and in optoelectronics.



Jonathan Coleman is the Professor of Chemical Physics and a researcher in the AMBER Research center at Trinity College Dublin. His research involves the production of nanomaterials and their applications from energy storage to sensing to electronics. He has published ≈ 350 papers in journals including Nature and Science and has been cited $\approx 55\,000$ times. He was recently listed by Thomson Reuters among the world's top 100 materials scientists and has collaborated with many companies including Hewlett-Packard, Intel, SAB Miller, Nokia-Bell Labs, and Thomas Swan.